Advancing helminth glycomics: structural specificity and immunogenicity of schistosomal and filarial glycans

Petralia, L.M.C.

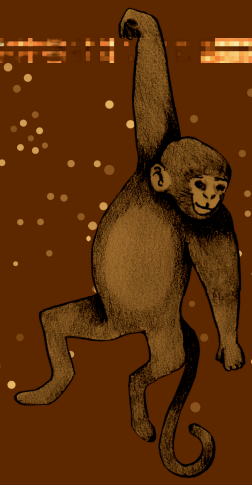

Chapter V.

Alteration of rhesus macaque serum *N*-glycome during infection with the human parasitic filarial nematode *Brugia malayi*

Laudine M. C. Petralia[1,2], Esrath Santha[1], Anna-Janina Behrens[1], D. Linh Nguyen[2], Mehul B. Ganatra[1], Christopher H. Taron[1], Vishal Khatri[3], Ramaswamy Kalyanasundaram[3], Angela van Diepen[2], Cornelis H. Hokke[2] and Jeremy M. Foster[1]

Scientific Reports, 2022

PMID: 36131114

DOI: 10.1038/s41598-022-19964-1

[1] Division of Protein Expression & Modification, New England Biolabs, Ipswich, MA, USA
[2] Department of Parasitology, Leiden University – Center of Infectious Diseases, Leiden University Medical Center, Leiden, The Netherlands
[3] Department of Biomedical Sciences, University of Illinois College of Medicine at Rockford, Rockford, IL, USA

Abstract

Serum *N*-glycan profiling studies during the past decades have shown robust associations between *N*-glycan changes and various biological conditions, including infections, in humans. Similar studies are scarcer for other mammals, despite the tremendous potential of serum *N*-glycans as biomarkers for infectious diseases in animal models of human disease and in the veterinary context. To expand the knowledge of serum *N*-glycan profiles in important mammalian model systems, in this study, we combined MALDI-TOF-MS analysis and HILIC-UPLC profiling of released *N*-glycans together with glycosidase treatments to characterize the glycan structures present in rhesus macaque serum. We used this baseline to monitor changes in serum N-glycans during infection with *Brugia malayi*, a parasitic nematode of humans responsible for lymphatic filariasis, in a longitudinal cohort of infected rhesus macaques. Alterations of the HILIC-UPLC profile, notably of abundant structures, became evident as early as 5 weeks post-infection. Given its prominent role in the immune response, contribution of immunoglobulin G to serum *N*-glycans was investigated. Finally, comparison with similar *N*-glycan profiling performed during infection with the dog heartworm *Dirofilaria immitis* suggests that many changes observed in rhesus macaque serum *N*-glycans are specific for lymphatic filariasis.

Introduction

Glycosylation is the most highly prevalent and structurally diverse post-translational modification of serum proteins. With the exception of albumin, all abundant proteins present in serum are glycosylated[1], with the glycan moieties imparting a plethora of biological functions[2]. Glycosylation and variation thereof are determined by many factors such as glycosyltransferase gene expression levels, availability of nucleotide sugar donors, transit time through the endoplasmic reticulum and Golgi, and accessibility of each *N*-linked glycosylation site[1]. However, extensive characterization of *N*-linked glycosylation profiles of human serum by mass spectrometry (MS) and ultraperformance liquid chromatography (UPLC)[1,3–6] have demonstrated the serum *N*-glycan profile of individuals to be generally highly stable[7], although influenced by phenomena such as gender, ethnicity and aging[8,9]. Similarly, many studies involving multiple patient serum samples, have correlated specific changes in the type or abundance of serum *N*-glycans with different pathological conditions. As such, glycoprofiling for diagnostic serum glycan biomarkers has become an intense research focus for numerous diseases, most notably various cancers[10–13], but extending to other conditions including cardiovascular disease and diabetes[14], rheumatoid arthritis[15], Crohn's disease and ulcerative colitis[16], congenital diseases[17,18], and liver fibrosis[19]. In addition, subtle changes in the glycosylation of immunoglobulin G (IgG), the most abundant serum glycoprotein, can dramatically affect its ability to elicit effector functions[20–22]. Since IgG is readily purified from serum, it has also been subjected to detailed glycoprofiling[23–27] and IgG *N*-glycans have proven effective biomarkers for a plethora of disease states[22]. Surprisingly, only a few studies have examined the IgG glycoprofiles from non-human species, yet these have revealed striking species-specific differences in both the nature and abundance of the appended *N*-glycans[28–30]. An even sparser literature exists on glycoprofiling of whole serum from other mammals[31,32], despite the fact that many species have huge veterinary or agricultural value or serve as animal models in biomedical research.

Rhesus macaques (*Macaca mulatta*) have a rich history of use as a non-human primate model in multiple areas of biomedical research including successful vaccine development (*e.g.* smallpox and polio), evaluation of monoclonal antibody therapies for various conditions and infectious diseases, as well as drug discovery[33,34]. However, extrapolation of preclinical findings from macaques to humans can be compromised when subtle differences in biology exist. For example, interspecies differences between immunoglobulins and their Fc receptors raise questions about the suitability of macaques for development of human antibody therapies and vaccines, and the extent to which data from animal trials can be translated clinically[33,35,36]. Nonetheless, as of today, studies of rhesus macaque glycoconjugates have been limited to IgG *N*-glycans[28,37].

One of many human diseases for which rhesus macaque have been used as an animal model is lymphatic filariasis (LF)[38,39], a chronic, debilitating neglected tropical disease caused by several species of filarial nematodes. *Wuchereria bancrofti* (*W. bancrofti*), *Brugia malayi* (*B. malayi*) and *Brugia timori* (*B. timori*) are responsible for LF in humans. They infect over 50 million people worldwide, with about 36 million people showing the severe clinical pathologies of elephantiasis and hydrocele[40]. Adult worms live in the lymphatic system for up to 10 years where ovoviviparous females produce millions of microfilarial larvae that enter the peripheral circulation and can be acquired by blood-feeding mosquitos. Diagnosis is predominantly through cumbersome microscopic detection of microfilariae in blood or using the more convenient immunochromatographic strip tests, although limitations of these tests have also been reported[41,42]. Disease control is through vector control strategies and through repeated mass drug administration to endemic communities, which is not ideal due to the limited effect of the few available drugs on the long-lived adult worms, suboptimal treatment responses and contraindication in certain geographic areas where *Loa loa* is co-endemic[43–45]. Thus, further research into novel drug targets and diagnosis tools is needed to reach the World Health Organization elimination target as part of the NTD roadmap for 2030[46]. Most research directed at developing a vaccine, new therapies or diagnostics for LF employ *B. malayi* since this is the only filarial nematode of humans that can be readily maintained in laboratory animals (Mongolian gerbil) as well as cats and primates. Rhesus macaques in particular have shown high similarities with humans in terms of lymphatic pathology and immune responses[38,39]. However, application of serum or IgG glycoprofiling for infectious diseases has focused mostly on infection with viral or bacterial pathogens[22,47] with very few studies addressing infections with eukaryotic parasites such as protozoa[48–50] or metazoan flatworms and nematodes[48,51,52].

The present study describes a comprehensive characterization of *N*-glycans from rhesus macaque whole serum and purified IgG using matrix-assisted laser desorption/ionization time of flight mass spectrometry (MALDI-TOF-MS) in combination with orthogonal glycan sequencing techniques. We also present the *N*-glycan profiles of both serum and IgG of healthy rhesus macaques using hydrophilic interaction chromatography with ultra-performance liquid chromatography (HILIC-UPLC) coupled with fluorescence detection and MS. We used healthy macaque *N*-glycan profiles as a baseline for monitoring glycosylation changes in a longitudinal cohort of monkeys infected with the human filarial nematode *B. malayi,* that ranges from pre-infection through to establishment of mature infection with adult worms and microfilarial production. We report significant temporal changes in the relative abundance of individual glycan structures as well as classes of *N*-glycan structures (e.*g.* galactosylation and sialylation) that arise due to parasitic infection. These glycan

profile changes expand our knowledge of the host response to filarial nematode infection and could provide insights into glycobiomarkers for LF infection in humans.

Materials and Methods

Reagents

All reagents were obtained from MilliporeSigma unless indicated otherwise. All enzymes were obtained from New England Biolabs (NEB).

Rhesus macaque serum samples

The cohort of longitudinal serum samples from rhesus macaques has been described previously[53]. Briefly, serum was first collected from 7 healthy monkeys and 4 of the animals were then infected by subcutaneous infection with 130 – 180 infective third stage larvae of *B. malayi*. Serum was sampled again at 5-, 12- and 15-weeks post-infection (wpi). All infected animals showed microfilariae in their blood by 12 wpi and impaired lymph flow when assessed at 16 wpi. Infection was confirmed by microscopic detection of microfilariae in blood. Details of disease progression and microfilariaemia for each animal are summarized in Table S3.

Ethical statement

Use of macaques and the experimental procedures performed in this study were reviewed and approved by The Institutional Animal Care and Use Committee (IACUC) at Bioqual Inc, Rockville, MA, USA and by the University of Illinois College of Medicine at Rockford, USA. Humane use of animals was performed according to the guidelines for the care and use of laboratory animals and with the rules formulated under the Animal Welfare Act by the U.S. Department of Agriculture in compliance with the Animal Research: Reporting of In Vivo Experiments (ARRIVE) guidelines. Ethical compliance, infection, treatment and animal maintenance have been reported in detail previously[53].

IgG purification from rhesus macaque serum

Aliquots of pre-infection serum from the 7 rhesus macaques were combined. IgG was purified from this serum pool using Protein G Spin Plates for IgG Screening (cat. #45204, Thermo Scientific, Pierce Biotechnology). 5 µL of serum (processed in technical duplicates) was diluted with MilliQ water (MQ, 5 µL) then mixed with binding buffer (10 µL, 0.1M NaHPO4 and 0.15 M NaCl, pH 7.2) and purified according to the manufacturer's instructions. Purified IgG samples were concentrated and buffer exchanged to MQ using Vivaspin® centrifugal devices (5000 Da MWCO; cat. #VS0111).

Samples were transferred to microfuge tubes, dried using a speed-vacuum centrifuge (Speedvac) and resuspended in MQ for subsequent *N*-glycan analysis. Protein concentration was estimated by absorbance measurement using Nanodrop.

MALDI-TOF-MS analysis

N-*glycan release*

A starting amount of 5 µL of the healthy rhesus macaque serum pool or 50 µg of purified serum IgG were mixed with PBS to reach a total volume of 100 µL. Samples were adjusted to 1.3% SDS and 0.1% β-mercaptoethanol. Denaturation was performed at 95°C for 10 min. After cooling, Nonidet P-40 was added (1.3% final concentration). *N*-linked glycans were released from glycoproteins using Peptide-N-glycosidase (PNGase) F (17 mU) for 24 h at 37°C. Released *N*-glycans were subsequently purified on octyldecylsilane (C18) cartridges (#7020-03 BAKERBOND® spe™, JT Baker®, Phillipsburg, NJ) equilibrated sequentially with acetronitrile (ACN), 60% ACN containing trifluoroacetic acid (TFA, 0.1%) and MQ. Samples were mixed with 1 mL of MQ and applied to the C18 columns which were washed with 10% ACN followed by MQ. The column flow-throughs containing the carbohydrates were applied to a carbon column (Supelclean™ ENVI-Carb SPE) previously equilibrated sequentially with ACN, 50% ACN containing 0.1% TFA and MQ. Columns were washed with MQ and glycans were eluted with 25% ACN followed by 50% ACN containing 0.1% TFA. Collected *N*-glycan samples were split in two and dried down using a Speedvac. One half was redissolved in 50 µL MQ and directly labeled with anthranilic acid (2-AA), while the other half was subjected to a linkage-specific sialic acid derivatization prior to 2-AA labeling.

Ethylation and amidation

Linkage-specific derivatization of the sialic acids by ethyl esterification was essentially performed according to a previously developed protocol[54,55]. Briefly, the dried *N*-glycan eluates were first redissolved in 3 µL of MQ, then, 60 µL of freshly made ethylation reagent consisting of a mixture of N-(3-Dimethylaminopropyl)-N'-ethylcarbodiimide hydrochloride and hydroxybenzotriazole (both at 0.25 M) in ethanol were added. Ethyl esterification was performed for 30 min at 37°C. 12 µL of 28% ammonium hydroxide was added to the reaction and incubation continued for a further 30 min at 37°C. Samples were dried down and redissolved in 30 µL of MQ.

Anthranilic acid labeling

The derivatized glycans (ethylated, amidated) and the unmodified glycans from carbon column eluates both separately resuspended in MQ as described above were mixed

with an equal volume of 2-AA labeling mix. 2-AA labeling mix was prepared by diluting 2-AA to a 48 mg/mL concentration and 2-picoline-borane complex to a 107 mg/mL concentration in DMSO:acetic acid (AcOH) (10:3). Labeling reactions were performed at 65° for 2 h.

Sample clean-up

Derivatized *N*-glycans were cleaned up using cotton HILIC solid phase extraction (SPE) following previously published methods[54,56] with the following modifications. 20 µL pipette-tips packed with 3 mm cotton thread (180 µg, Pipoos, Utrecht, Netherlands) were washed with MQ and 85% ACN. Samples were loaded onto the tips by pipetting up and down 30 times before sequential washes with 85% ACN-0.1% TFA and 85% ACN. Glycans were eluted with 30 µL of MQ pipetted up and down 10 times through the cotton HILIC resin. For the remainder of the glycan samples (unmodified glycans), excess 2-AA labeling reagent was removed by SPE using Biogel P10 (#1504144 Bio-Rad, Hercules, CA). 200 µL of a 100 mg/mL solution of Biogel P10 in 10% ACN was loaded into the wells of a 96-well filter plate on top of a vacuum manifold device. The resins were washed sequentially with MQ and 80% ACN. Samples were brought to 75% ACN and loaded onto the resin. Following 4 washes with 80% ACN, samples were eluted from the Biogel P-10 twice with 200 µL of MQ. Samples were dried using a Speedvac and resolubilized in MQ. An additional clean-up step using C18 ZipTips (#ZTC18S096) was performed according to manufacturer's instructions except for the final step, where the glycans were eluted in 50% ACN, 0.1% TFA mixed with 2,5-dihydroxybenzoic acid (DHB), at a concentration of 10 mg/ml (#8201346, Bruker Daltonics, Bremen, Germany). This facilitated direct sample loading to a 384-well steel polished target plate for MS analysis.

MALDI-TOF-MS and MALDI-TOF-MS/MS

2-AA-labeled *N*-glycans were analyzed using MALDI-TOF-MS performed using an UltrafleXtreme® mass spectrometer (Bruker Daltonics) equipped with a 1 kHz Smartbeam II laser technology and controlled by the FlexControl 3.4 Build 119 software (Bruker Daltonics). Ethylated and amidated *N*-glycans, eluted in MQ during HILIC clean-up, were mixed in a 1:2 ratio with DHB matrix at a concentration of 20 mg/ml in 30% ACN and spotted onto a 384-well steel polished target plate for MALDI-TOF-MS analysis, while 2-AA-labeled *N*-glycans processed through C18 ZipTips were directly spotted onto the target plate as described above. All spectra were recorded in the negative-ion reflectron mode using Bruker® peptide calibration mix (#8206195, Bruker Daltonics) for external calibration. Spectra were obtained over a mass window of m/z 700 – 4000 with ion suppression below m/z 700 for a minimum of 20,000 shots (2000 Hz) obtained by manual selection of "sweet spots". The FlexAnalysis 3.4 Build 76

software was used for data processing including smoothing of the spectra (Savitzky Golay algorithm, peak width: m/z 0.06, 1 cycle), baseline subtraction (Tophat algorithm) and manual peak picking. Known non-glycan peaks such as glucose polymers were excluded. Possible compositions of deprotonated masses of the selected peaks were assigned using the GlycoPeakfinder® tool of the GlycoWorkBench software [57] (http://www.eurocarbdb.org/applications/ms-tools, Version 3, June 2007) allowing the following residues within the search engine: 2-20 hexoses and N-acetylhexosamines, 0-5 deoxyhexoses (Fucoses), 0-4 *N*-glycolylneuraminic acid (Neu5Gc) and 0-4 *N*-acetylneuraminic acid (Neu5Ac). Linkage-specific derivatization of sialic acids resulted in mass differences of sialic acids compared to their unmodified variants of 291.10 Da for Neu5Ac and 307.09 Da for Neu5Gc. Derivatization of α2,6-linked sialic acids results in an increase of +28.031 Da upon esterification[55]. Thus, we included the increment masses of 319.127 Da for α 2,6-linked Neu5Ac and 335.307 Da for α2,6-linked Neu5Gc. In addition, amidation of α2,3-linked sialic acids yields side products showing a mass difference of −0.984 Da corresponding to increment masses of 290.085 Da for α2,6-linked Neu5Ac and 306.249 Da for α2,6-linked Neu5Gc. The 2-AA label was also taken into account as a fixed reducing-end modification for composition assignment. Compositions were narrowed and confirmed by combining information derived from HILIC-UPLC analysis, glycosidase digestions (see below) and tandem MS (MS/MS). MS/MS was performed on underivatized, 2-AA-labeled rhesus macaque IgG *N*-glycans. Selected ions were subjected to fragmentation analysis by MALDI-TOF/TOF using the UltrafleXtreme® mass spectrometer in negative-ion mode.

HILIC-UPLC profiling of *N*-glycans

We used HILIC-UPLC to monitor the *N*-glycan profiles of rhesus macaques pre- and post-infection with *B. malayi* using the longitudinal set described above. We released serum *N*-glycans for each of the animals pre-infection (n = 7) to generate a baseline and for each of the animals subsequently infected with *B. malayi* (n = 4) at 5, 12 and 15 wpi. Each individual sample was processed separately, with technical duplicates to assess potential changes of the *N*-glycan profile upon infection. *N*-glycans in all samples were released and labeled with procainamide using the protocol optimized and described previously[32]. Briefly, *N*-glycan release was performed using Rapid™ PNGase F (#P0710) and directly followed by labeling. 12 µL of acidified procainamide (550 mg/mL procainamide stock solution in DMSO mixed with AcOH; 8:1 ratio) and 9 µL of sodium cyanoborohydride (200 mg/mL in MQ) were added to each deglycosylation reaction. Excess labeling reagent was then removed using HILIC clean-up plates (SNS-HIL, The Nest Group Inc., Southborough, MA, USA). The procainamide-labeled *N*-glycans were analyzed using HILIC-UPLC as described[32,51]. Briefly, a Waters Acquity H-class instrument (Waters Corp., Milford, MA, USA) composed of a binary solvent manager, a sample manager, a fluorescence detector (excitation wavelength 310 nm; detection

wavelength 370 nm) and a QDa mass detector (settings: positive mode; target sampling rate: 10 point/sec; gain: 1; capillary voltage: 1.5 kV; probe temperature: 600 °C) was used for UPLC profiling. Glycans were separated using an Acquity BEH Amide Column (130 Å, 1.7 µm, 2.1 mm x 150 mm; Waters Corp.) with 50 mM ammonium formate, pH 4.4 as solvent A and acetonitrile as solvent B using a linear gradient of 70 % to 53 % solvent B at 0.56 ml/min for 25 min. Data from both the fluorescence and the mass detectors was acquired, processed and analyzed using Empower 3 software (Waters Corp.). Glucose units (GU) were assigned using a procainamide-labeled dextran ladder (cat. #CPROC-GHP-30, Ludger, Abingdon, UK) and a fifth-order polynomial distribution curve.

HILIC-UPLC data analysis and statistics

Peak areas of HILIC-UPLC spectra quantified using Empower 3 were exported and normalized to an arbitrary identical total peak area value of 10,000,000 for each spectrum. Statistical analysis was performed using the software R (version 4.0.0 Patched). The MSstats package[58] (10.18129/B9.bioc.MSstats) was used to assess significant changes between time-points in the course of disease progression as described previously[51]. We performed this analysis on the longitudinal cohort consisting of the four animals described above. More specifically, for each animal, HILIC-UPLC profiles obtained at 5, 12 and 15 wpi were compared to their corresponding baseline profiles.

Glycosidase digestions of released and labeled *N*-glycans

Released and labeled *N*-glycans from the healthy rhesus macaque serum pool and from rhesus macaque IgG were further characterized by enzymatic digestions. Sequential enzymatic digestions were performed using a panel of exoglycosidases. 8 µL of the serum *N*-glycan pool and 2 µL of the IgG *N*-glycans were digested with 1 µL of one or more exoglycosidase(s) to create a sequential digestion panel. For this purpose, α2-3,6,8,9 Neuraminidase A (cat. #P0722), α1-2,4,6 Fucosidase O (cat. #P0749), β1-4 Galactosidase S (cat. #P0745) and β-N-Acetylglucosaminidase S (cat. #P0744) were used. 1 µL of recommended buffer was added to each reaction and final reaction volumes were adjusted to 10 µL with MQ. Similarly, non-sequential digestions were performed by mixing 2 to 8 µL of the *N*-glycan samples with one of the following glycosidases in recommended amount and buffer: α2-3 Neuraminidase S (cat. #P0743), α1-2,4,6 Fucosidase O (#P0749), α 1-3,4,6 Galactosidase (#P0747), β1-4 Galactosidase S (#P0745) and β-N-Acetylglucosaminidase S (#P0744) or Endoglycosidase H (#P0702). Glycosidase sources and reaction conditions are further detailed in Table S7. Undigested controls consisting of 2 to 8 µL of sample mixed with digestion reaction buffer and MQ were included for each experiment. Digestion

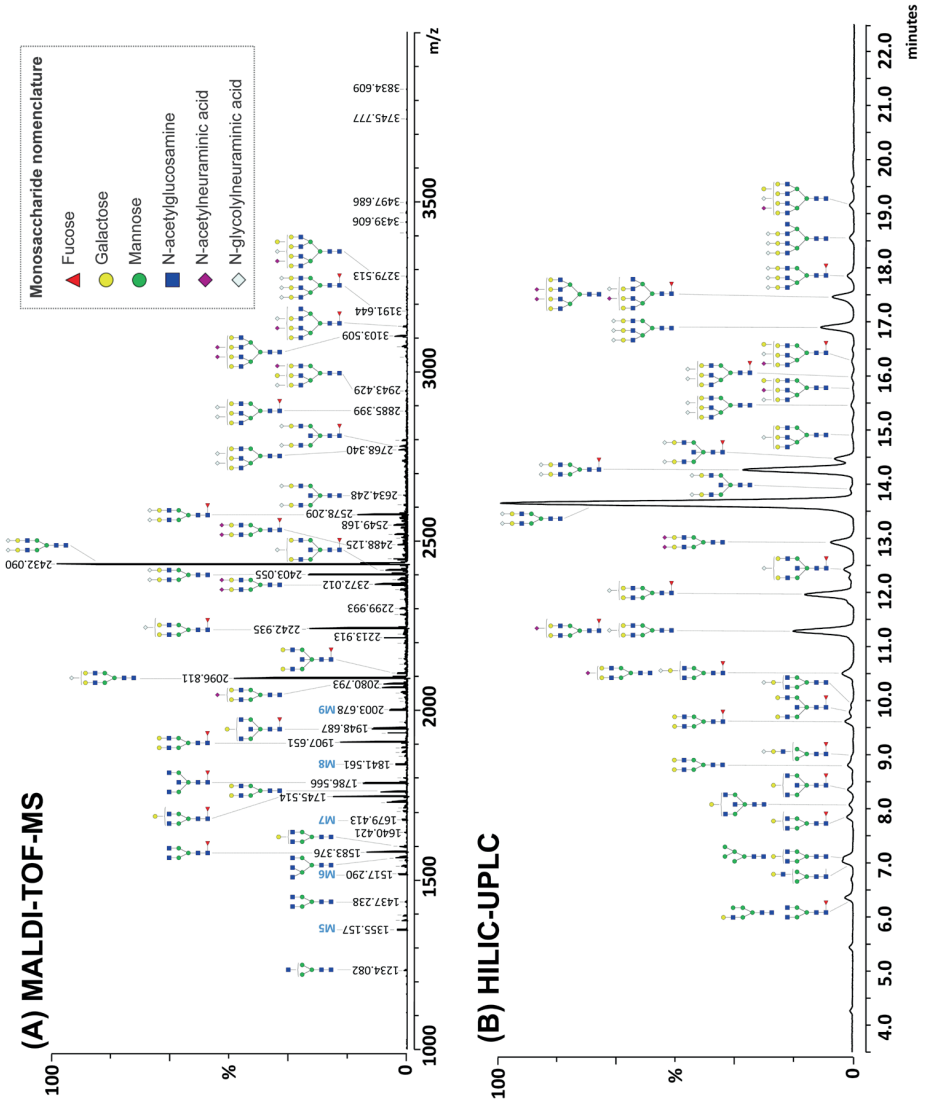

Figure 1. MALDI-TOF-MS analysis and HILIC-UPLC profiling of rhesus macaque serum *N*-glycans
PNGase F-released glycans from rhesus macaque serum glycoproteins were labeled with 2-AA and analyzed by MALDI-TOF-MS (A) or labeled with procainamide and analyzed using HILIC-UPLC (B). *N*-glycans were subjected to linkage-specific derivatization of the sialic acids by ethyl esterification prior to labeling with 2-AA for MALDI-TOF-MS. MALDI-TOF-MS signals were measured in negative ion reflectron mode and are labeled with monoisotopic masses (see **Table S1** and **Figure S1**). *N*-glycan structures were assigned by combining data from both approaches and by using glycosidase digestions (see **Figure S2** and **S3**). Proposed structures resulting from this analysis are depicted for selected peaks using the Consortium for Functional Glycomics (CFG) nomenclature (see symbol key inset). M5-9 designate mannosylated *N*-glycans with 5 to 9 mannose residues.

reactions were incubated overnight at 37°C prior to enzyme clean-up. MultiScreen® 96 well filter plates (cat. #MAIPS4510) containing 0.45 µm hydrophobic high protein binding immobilon-P membrane was used as recommended for purification of the procainamide-labeled *N*-glycans while C18 Zip-tips were used as detailed above for purification of 2-AA-labeled *N*-glycans. Finally, digested *N*-glycan samples and undigested controls were analyzed using either HILIC-UPLC for procainamide-labeled *N*-glycans or MALDI-TOF-MS for 2-AA-labeled *N*-glycans as described above.

Results

MALDI-TOF-MS and HILIC-UPLC based characterization of rhesus macaque serum and IgG

We characterized the *N*-glycans isolated from total serum glycoproteins of a pool of seven rhesus macaques and those from purified IgG using a combination of techniques including MALDI-TOF-MS and HILIC-UPLC. First, *N*-glycans were released from rhesus macaque serum glycoproteins, labeled with 2-AA and analyzed by MALDI-TOF-MS. This allowed the initial identification of 45 different serum *N*-glycan structures (**Figure S1.A**). An additional 38 sialylated *N*-glycan structures, mostly in the higher mass range, were detected with a similar analysis including a linkage-specific derivatization and stabilization of sialic acid using ethyl esterification[54,55] (**Figure 1.A** and **Figure S1.B**). In total, 83 different *N*-glycan structures could be characterized. This number included many isomeric forms differing only by the linkages of the terminal sialic acids, as revealed using the specific derivatization that permits discrimination of α2-3 and α2-6 linkages. These 83 structures were represented by 65 different *N*-glycan compositions. Structural assignment was performed by digesting sequentially and individually the rhesus macaque serum *N*-glycans using the broad Neuraminidase A, Fucosidase O, β1-4 Galactosidase S and β-N-Acetylglucosaminidase S (**Figure S2 and S3**). Using these enzymes sequentially, we reduced the *N*-glycans to their tri-mannosylated core and demonstrated the presence of a large variety of structures ranging from short, truncated *N*-glycans to multi-antennary complex *N*-glycans. Structures with up to four antennae (A1 to A4) were confirmed upon digestion with a mix of Neuraminidase A, Fucosidase O and β1-4 Galactosidase S. These antennae were extended with β-linked galactoses and sialic acids (**Figure S2.A**).

In parallel, we used a previously validated HILIC-UPLC profiling workflow to analyze PNGase F-released and procainamide-labeled *N*-glycans[32] (**Figure 1.B**). Forty-three distinct integratable peaks (referred to as “glycopeaks” in the following sections) were identified and correlated with the serum profile (**Figure S1.C**). *N*-glycan structures comprising the glycopeaks were characterized using MS data obtained from the QDa mass detector linked to the UPLC instrument (see Methods) in combination

with glycosidase digestions (F**igure S2.B**). Data from these orthogonal approaches were highly complementary, with only two minor glycopeaks from the HILIC-UPLC spectra not matching any MALDI-TOF-MS data. Similarly, 11 structures detected by MALDI-TOF-MS (mostly minor ions generated by short, truncated or high-mannose *N*-glycans) were not observed in HILIC-UPLC profiles.

Peak areas were quantified from HILIC-UPLC spectra and the relative abundance of each glycopeak compared to the total peak area of each spectrum. The most abundant *N*-glycan observed in rhesus macaque serum was biantennary $A2G2S_{Gc}2$ which accounted for almost 48% of the total *N*-glycan pool. It was followed by the core-fucosylated version of the same structure ($F(6)A2G2S_{Gc}2$) which accounted for over 10% (Table S1). Due to the instability and ionization bias experienced by sialylated glycan species during MALDI-TOF-MS analysis[54,55,59], the major ion in the MALDI-TOF-MS spectra of underivatized *N*-glycans corresponded to $A2G2S_{Gc}1$ (*m/z* 2067.927 $[M - H]^-$) (**Figure S1**). This was corrected using the linkage-specific derivatization method, where $A2G2S_{Gc}2$ (2432.090 $[M - H]^-$) appeared as the most abundant ion species. Notably, this analysis allowed for identification of Neu5Ac in many *N*-glycans (*e.g. m/z* 2372.012, 2488.125, 3103.509 $[M - H]^-$, **Figure 1**), although this form of sialic acid was less prominent than Neu5Gc. Using HILIC-UPLC, we estimated the proportion of *N*-glycans carrying Neu5Ac to be ~6% of the total glycan pool while 81% was sialylated with Neu5Gc. About 4% were complex *N*-glycans with high *m/z* (2800-4000 range) and late HILIC-UPLC retention times that possessed both sialic acid forms (*e.g. m/z* 3103.509, 3279.513 $[M - H]^-$, and glycopeaks 35 at 17,4 min and 38 at 19,1 min, **Figure 1**).

In addition to the sequential glycosidase digestion panels (**Figure S2**), complementary digestions with individual enzymes were also performed (**Figure S3**) to confirm serum *N*-glycan structural assignment. Notably, comparison of digestions with the specific α2-3 Neuraminidase S with broad-specificity α2-3,6,8,9 Neuraminidase A using HILIC-UPLC analysis showed that although the majority of the sialic acids were α2-6 linked, a significant proportion were α2-3 linked, supporting the assignments made by MALDI-TOF-MS analysis with sialic acid linkage-specific derivatization. Thus, by combining the glycosidase digestion results with HILIC-UPLC and MALDI-TOF-MS analysis, a comprehensive structural assignment of rhesus macaque serum *N*-glycans was obtained (**Figure 1**). Detailed structural assignments and MALDI spectra annotated with glycopeak numbering are presented in **Figure S1** and **Table S1**.

An identical analysis was performed on IgG purified from the rhesus macaque pool of sera (**Figure 2**). Using MALDI-TOF-MS, 26 *N*-glycan structures were identified that were further extended to 43 with the additional step of ethyl esterification of sialic acids (**Figure S4**). In addition, 19 glycopeaks were observed in the HILIC-UPLC profile that correlate with 30 of the *N*-glycans identified using MALDI-TOF-MS, with the

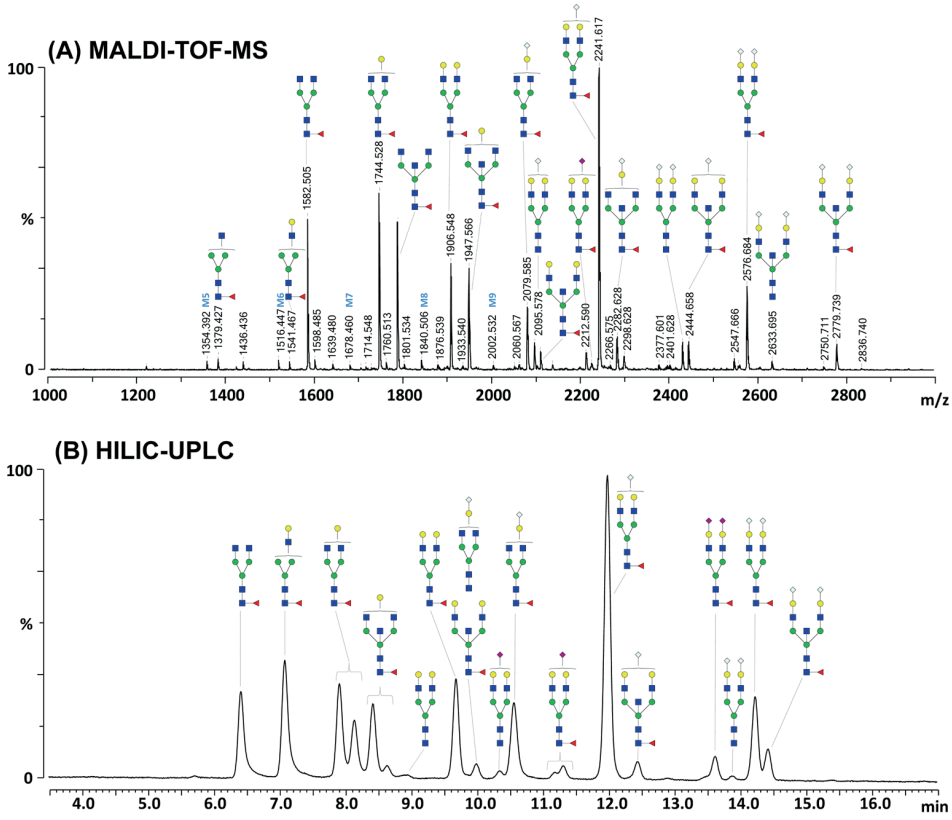

Figure 2. MALDI-TOF-MS analysis and HILIC-UPLC profiling of rhesus macaque IgG *N*-glycans
PNGase F-released glycans from purified rhesus macaque IgG were labeled with 2-AA and analyzed by MALDI-TOF-MS (A) or labeled with procainamide and analyzed using HILIC-UPLC (B). *N*-glycans were subjected to linkage-specific derivatization of the sialic acids by ethyl esterification prior labeling with 2-AA for MALDI-TOF-MS. MALDI-TOF-MS signals were measured in negative ion reflectron mode and are labeled with monoisotopic masses (see **Table S2** and **Figure S4**). *N*-glycan structures were assigned by combining data from both approaches and by using glycosidase digestions as well as MALDI-TOF-MS/MS (see **Figure S5** and **S6**). Proposed structures resulting from this analysis are depicted using the Consortium for Functional Glycomics (CFG) nomenclature (see symbol key inset in **Figure 1**). M5-9 designate mannosylated *N*-glycans with 5 to 9 mannose residues.

exception of glycopeak #16 (**Table S2**). This resulted in a total of 13 *N*-glycan structures being identified by MALDI-TOF-MS analysis that were not detected by HILIC-UPLC profiling (due to their lower abundance).

These *N*-glycans were further characterized using sequential and individual glycosidase digestion. This analysis revealed that IgG *N*-glycans were comprised of structures bearing terminal sialic acids, terminal β-linked galactoses, α-linked fucoses, or were mannosylated structures (**Figure S5** and **S6**). Finally, tandem MS

using MALDI-TOF-MS/MS confirmed the presence of bisecting GlcNAcs on some structures, consistent with prior observations on rhesus macaque IgG *N*-glycans[28,37]. Fragmentation profiles of selected ions with theoretical *m/z* 1436.53 and 1639.61 [M – H]$^-$ from IgG *N*-glycans both indicate the presence of bisecting GlcNAc (**Figure S6.B**).

N-glycan profiles of serum and IgG from human and rhesus macaques exhibit differences

Exoglycosidase digestions combined with HILIC-UPLC analysis permitted quantification of the following *N*-glycan categories in rhesus serum: galactosylated (*N*-glycans bearing at least one terminal unsubstituted galactose), fucosylated (fucose-containing *N*-glycans), sialylated (*N*-glycans having at least one antenna terminated by sialic acid) and mannosylated (oligomannosidic or hybrid *N*-glycans). Analysis of human serum *N*-glycans was previously conducted using the same workflow[32], allowing a direct comparison. Most rhesus macaque serum *N*-glycans are sialylated, with over 91% of the UHPLC profile area being sensitive to α2-3,6,8,9 Neuraminidase A treatment (**Figure 3.A**). This percentage appeared higher than observed for humans (~87%). The majority of the sialic acids in rhesus macaque serum *N*-glycans are Neu5Gc. This is consistent with the presence of a putative functional CMP-*N*-acetylneuraminic acid hydroxylase (CMAH) gene – the only enzyme capable of synthesizing Neu5Gc by hydroxylation of Neu5Ac[60–62] – in rhesus macaques[63]. This gene is deactivated in a number of lineages including that leading to humans[64]. Thus, while the major structure in human is A2G2S2, the major structure in rhesus macaques is A2G2S$_{Gc}$2. Using Fucosidase O digestion, we determined that around 30% of the total *N*-glycan serum pool is fucosylated in rhesus macaques while it was found to be slightly less than 24% in humans. The abundance of FA2G2S$_{Gc}$2 in rhesus macaques largely contributes to this overall higher fucosylation, since the ratio between the A2G2S$_{Gc}$2 and its fucosylated variant (FA2G2S$_{Gc}$2) in rhesus macaque is considerably lower than between A2G2S2 and FA2G2S2 in human. We also noted a smaller amount of agalactosylated *N*-glycans in rhesus macaque serum compared to human serum, which was particularly evident for the F(6)A2-containing glycopeak, while the proportion of galactosylated *N*-glycans was similar in both species at 20% of the total *N*-glycan pool. Digestions with β1-4 Galactosidase showed that all galactoses were β1-4 linked and this was confirmed by the absence of sensitivity to the broad-specificity α1-3,4,6 Galactosidase (**Figure S3**), consistent with the absence of α1,3 galactosylation in the common ancestor of old world primates due to the loss of α1,3 galactosyltransferase[65]. Finally, a small portion (around 3%) of mannosidic and hybrid *N*-glycans, which have also been found in humans, was revealed using Endoglycosidase H (**Figure S3**).

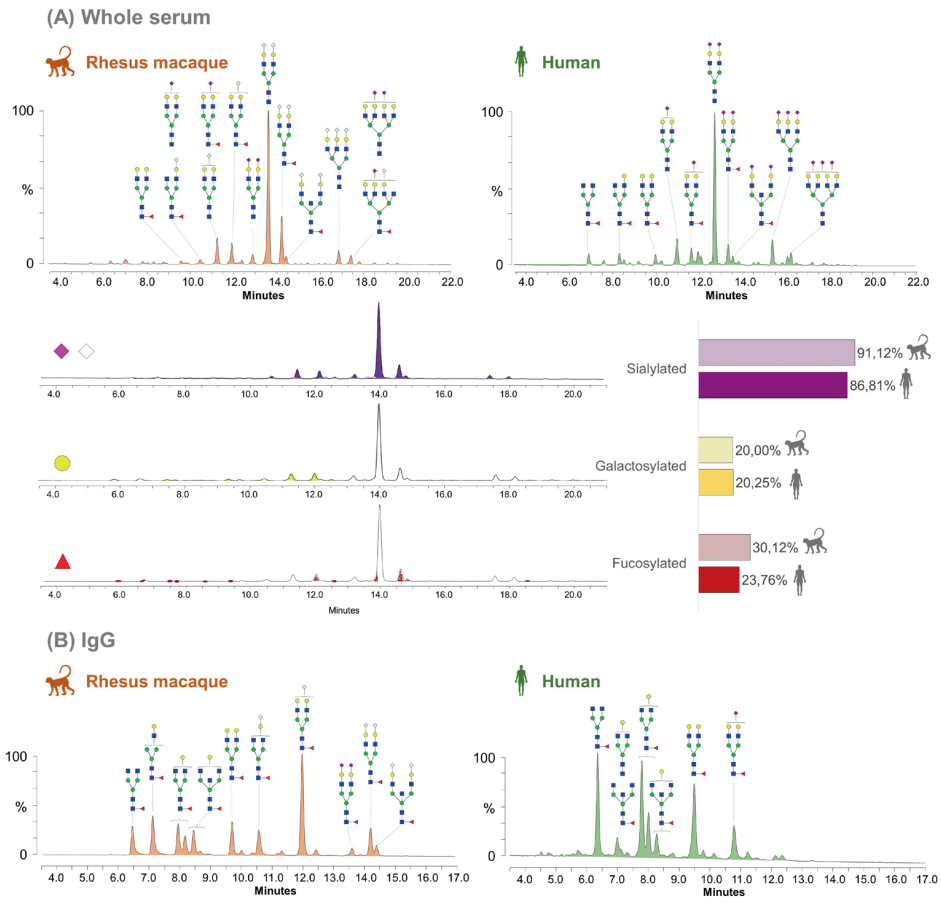

Figure 3. Comparison of rhesus macaque and human HILIC-UPLC profiles of serum (A) and IgG (B) *N*-glycans

HILIC-UPLC spectra of rhesus macaque (left) and human (right) are shown for both serum (A) and IgG (B). *N*-glycan structures found in the 10 major glycopeaks (based on peak areas) are depicted using the CFG nomenclature (see inset in **Figure 1**). Quantification of glycan classes in rhesus macaque serum was determined before and after digestion with α2-3,6,8,9 Neuraminidase A for sialylated structures (purple and grey diamonds), β1-4 Galactosidase S for structures carrying terminal galactose (yellow circle) and with Fucosidase O for core-fucosylated structure (red triangle). Results were compared with similar quantification data conducted previously on human serum[32] and are shown on the bar chart on the right.

In accordance with previous studies[28,37], we also found the IgG *N*-glycans of rhesus macaque to be substantially different from human IgG (**Figure 3.B**). Although IgG profiles from both species share many, largely core-fucosylated, *N*-glycan structures, the relative proportion of these *N*-glycans differed considerably. Indeed, the rhesus macaque IgG profile is dominated by the *N*-glycan structure F(6)A2G2S_{Gc}1, while the agalactosylated (F(6)A2) and galactosylated (F(6)A1-2G1-2) structures, which

constitute the majority of human IgG *N*-glycosylation, appear in markedly lower amounts on rhesus macaque IgG. Thus, rhesus macaque IgG exhibits a significantly higher abundance of larger sialylated *N*-glycans compared to human, which differentially impacts the contribution of IgG *N*-glycans to the total serum *N*-glycoprofile. Indeed, in human, IgG *N*-glycans are nearly all smaller than A2G2S2 and, thus, do not contribute to the most abundant complex *N*-glycan structures[1], while in rhesus macaque, IgG *N*-glycans contribute to FA2G2S$_{Gc}$2 and FA2(B)G2S$_{Gc}$2 (glycopeaks #25 and 26), two major sialylated *N*-glycans of the HILIC-UPLC serum profile. As for serum *N*-glycans, the vast majority of the IgG sialic acids were Neu5Gc. However, we detected a minor amount of the Neu5Ac form of sialic acid in several glycopeaks (**Figure 2** and **Table S2**) which has not been reported previously for rhesus macaques[28,37].

Finally, we also found bisecting GlcNAc which is a common feature in both species, but has been determined to be more prominent in rhesus macaques compared to humans[37]. Although we did not perform any quantitative analysis of bisecting GlcNAc-containing *N*-glycans, we detected them in a significant amount on rhesus macaque IgG (**Figure S5**). Presence of bisecting GlcNAc explains the S incomplete digestion of the structure FA2B (*m/z* 1639.506 $[M - H]^-$) using β-N-acetylglucosaminidase (residual peak *m/z* 1395.347 $[M - H]^-$).

Changes in serum *N*-glycosylation during the course of *B. malayi* infection

To study if infection with *B. malayi* affects serum *N*-glycosylation, we used the HILIC-UPLC workflow to monitor the profiles from a longitudinal set of rhesus serum samples over the course of their infection with this filarial nematode. Firstly, serum samples from 7 different healthy animals were analyzed separately with technical duplicates and yielded highly similar HILIC-UPLC profiles resulting in a stable baseline for the serum *N*-glycan profile of healthy rhesus macaques (**Figure S7** and **Table S4.A**). Secondly, serum was sampled from four of these rhesus macaques at 5, 12 and 15 wpi with *B. malayi* infective larvae (Materials and Methods section and **Table S3**). Again, serum *N*-glycans were analyzed using HILIC-UPLC for each individual animal, at each time-point, with technical duplicates (**Table S4.A**). To study the alteration of the *N*-glycan serum profile during the course of *B. malayi* infection, we used statistical analysis based on linear-mixed effect models[58], to compare the HILIC-UPLC profiles of individual animals from the longitudinal cohort at 5, 12 and 15 wpi to their corresponding pre-infection ones. Changes arose as early as 5 wpi when 17 glycopeaks showed significant differences in their relative peak area (in percentages) between infected and baseline time-points (adjusted p-value < 0,05). Alteration of serum *N*-glycosylation increased as the infection progressed, with 24 glycopeaks showing

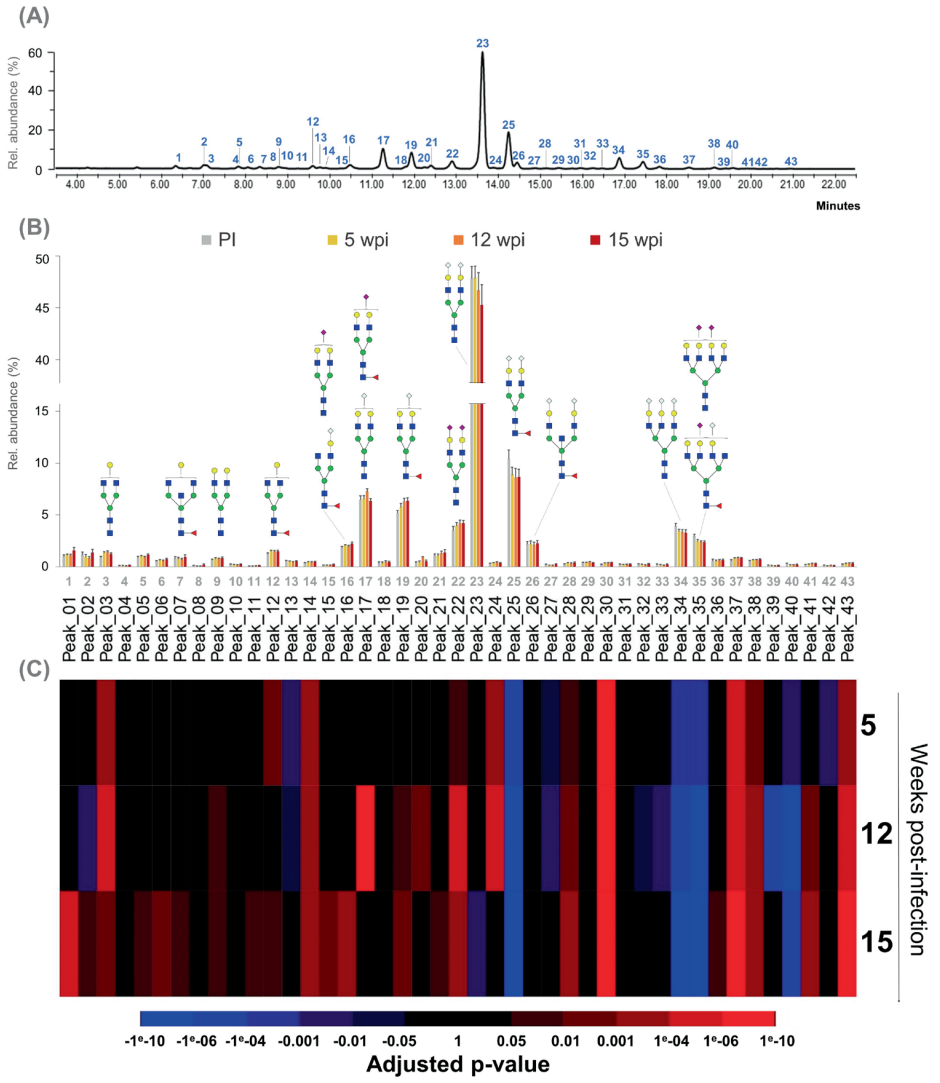

Figure 4. Changes in HILIC-UPLC profile of rhesus macaques serum *N*-glycans during infection with *B. malayi*

Quantification of individual peaks derived from HILIC-UPLC spectra was performed for 4 different animals at 4 different time-points namely pre-infection (PI), 5 weeks post infection (wpi), 12 wpi and 15 wpi (see **Table S4.A**). The HILIC-UPLC traces obtained at pre-infection for the 4 animals are overlaid in (A), and glycopeak numbering is indicated. Individual glycopeak areas were integrated and quantified at each of the time-points. Average of glycopeak relative abundance (Rel. abundance) for the 4 animals are shown on the bar graph (B) with standard error bars. The x-axis displays the peak numbers corresponding to the HILIC-UPLC profile. Using linear mixed-effect models, changes in the abundance of serum *N*-glycans during infection were assessed and results of the statistical analysis for each glycopeak are presented in the heatmap (C). Decrease in abundance (blue) and increase in abundance (red) is relative to baseline (pre-infection) for each time point see color key). Adjusted p-values can be found in **Table S4.B**. Selected glycan structures are represented using the CFG nomenclature (inset in **Figure 1**).

statistically significant changes in abundance at 12 wpi and 27 glycopeaks at 15 wpi. Many altered glycopeaks were abundant ones in the HILIC-UPLC profile with, for instance, the major glycopeak (#23 in the HILIC-UHPLC profile) that significantly decreased at 15 wpi or glycopeak #25 that showed a significant reduction as early as 5 wpi and continued until 15 wpi when compared to baseline. Interestingly, many of the early changes - either a decrease or increase in relative abundance - lasted up to 15 wpi as this was observed for 12 out of the 17 glycopeaks (**Figure 4** and **Table S4.B**). In addition, some noticeable changes became evident at 15 wpi, with a clear increase for many shorter glycan structures that appear early in the HILIC-UPLC profile (*e.g.* glycopeak #1, 2, 3, 5, 6, 7, 9 11, 12, 15, 16, 20) and a significant decrease for the most abundant serum *N*-glycan (glycopeak #23). Overall, the directionality of changes appeared to be consistent over the course of the infection, since only glycopeak #2 fluctuated (decrease at 12 wpi and increase at 15 wpi), while the relative abundance of all other glycopeaks that showed changes were consistently increased or decreased throughout the longitudinal study.

We also analyzed *N*-glycosylation of purified IgG from serum of all 4 infected monkeys at each time-point. In contrast, total IgG glycosylation in infected rhesus macaques did not show any significant changes in *N*-glycosylation over the course of infection (data not shown).

We next aimed to investigate trends within the main *N*-glycan classes present in rhesus macaque serum during infection. Structural assignment performed on the basis of exoglycosidase digestions allowed us to estimate the relative abundance of sialylated, fucosylated, galactosylated and mannosylated (oligomannosidic or hybrid) *N*-glycans at each time-point (**Figure 5** and **Table S5**). Unlike changes in individual *N*-glycan structures, the first significant changes in these broad *N*-glycan classes appear only at 12 wpi with an increase in both galactosylation and mannosylation. However, at 15 wpi this increase in galactosylated and mannosylated *N*-glycans appears to become more substantial (with p-values < 0.001) and is accompanied by a decrease in sialylated structures. This finding is in line with changes in individual glycans described above since structures eluting at the earliest retention times are mainly galactosylated and mannosylated. Thus, the increased abundance of these structures at 15 wpi and the decreased abundance of the major sialylated *N*-glycan likely explain the observed trends for the *N*-glycan classes.

Given that the main goal of performing such glycoprofiling studies is to identify potential glycan biomarkers of infection or disease, we decided to focus on changes in the most abundant *N*-glycan structures which constitute more promising targets for diagnostic application. Since we noticed a slightly higher technical variation for the smallest peaks in the profile and for those with the later retention times, we selected the 20 glycopeaks with areas larger than 0.5% of the total profile area and with a retention time less than 18 min in the HILIC-UPLC profile. The volcano plots

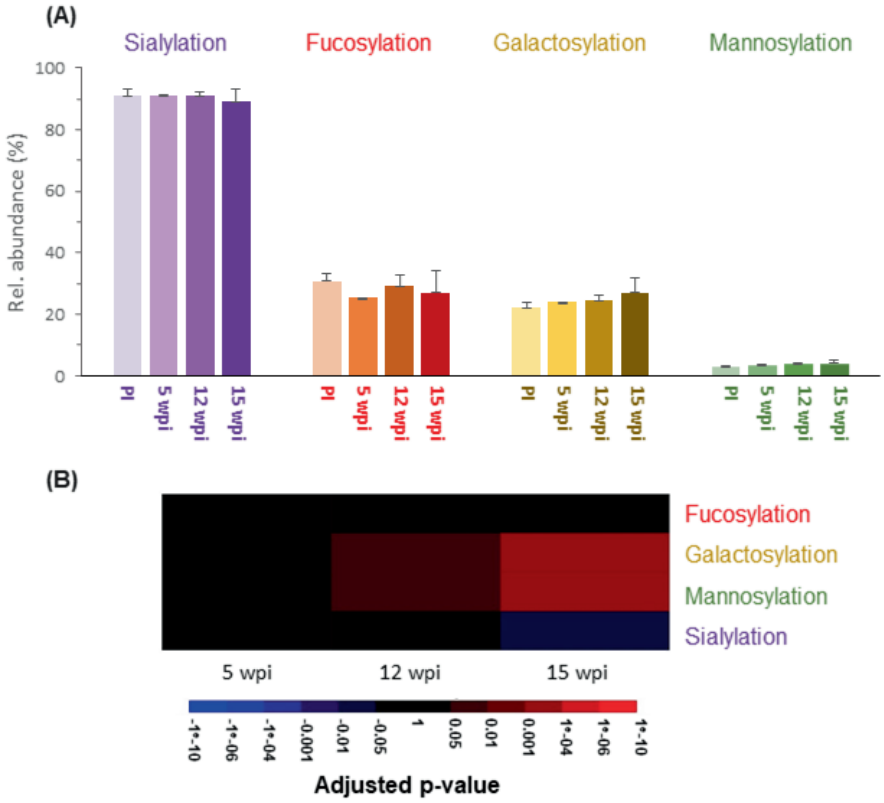

Figure 5. Changes in the major classes of rhesus macaque serum *N*-glycans during the course of infection with *B. malayi*

N-glycan content of each glycopeak in the UPLC profile was structurally characterized using a combination of UPLC-profiling, MALDI-TOF-MS and glycosidase digestions. Based on their glycan content, glycopeaks belonged to the following glycan classes: sialylated (purple), fucosylated (red), galactosylated (yellow) and/or mannosylated (green). Relative abundance (Rel. abundance) of each class of glycan was quantified by adding individual peaks areas belonging to the same class. This was done for each animal (n = 4) at each of 4 time-points: pre-infection (PI), 5 weeks post-infection (wpi), 12 wpi and 15 wpi. Results of this analysis are shown by the bar chart (A). The relative abundance of each glycan class was averaged for all animals and shown as percentages with standard deviation as error bars. Statistically significant changes in relative abundance of glycan classes in the course of the infection were estimated using linear mixed-effect models. Adjusted p-values can be found in **Table S5** and were used to generate the heatmap (B). Blue color indicates a decrease in abundance and red an increase.

summarizing the results of the statistical analysis performed on these peaks are shown in **Figure 6**. As previously seen when studying changes for the overall HILIC-UPLC profile, the number of glycopeaks showing statistical differences compared to healthy serum increased during infection. Thus, in this glycopeak selection, 7 peaks are significantly altered at 5 wpi, 10 at 12 wpi and 17 peaks at 15 wpi. Moreover, this was

accompanied by a noticeable increase in the negative log2 of the adjusted p-values. Interestingly, 6 out of the 7 glycopeaks showing differences as early as 5 wpi were either decreased (#13, 25, 34, 35) or increased (#3, 22) throughout the 3 time-points, supporting consideration of these glycan structures as potential biomarker candidates.

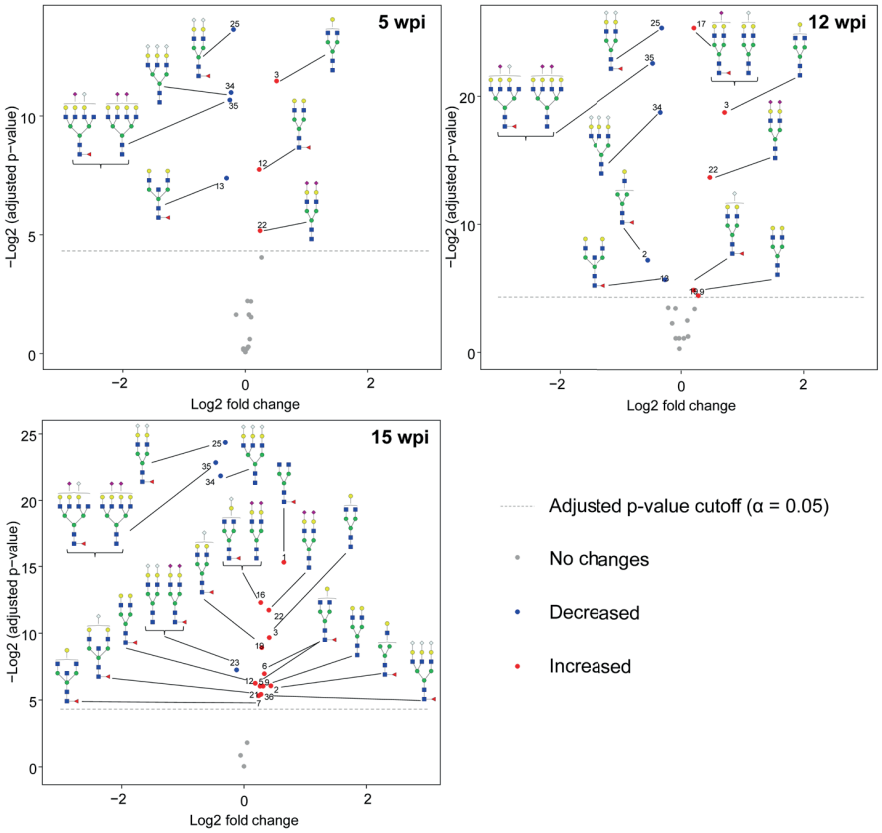

Figure 6. Changes in the major HILIC-UPLC glycopeaks of the rhesus macaque serum *N*-glycan profile upon infection with *B. malayi*

Glycopeaks from the HILIC-UPLC profiles of healthy rhesus macaque serum *N*-glycans with areas above 0.5% of the total profile area at baseline (pre-infection) were selected. Changes in the relative abundance of the 20 glycopeaks resulting from this selection were studied across infection by comparing the post-infections time-points: 5 (A), 12 (B) and 15 (C) weeks post-infection (wpi) - with pre-infection (baseline). Adjusted p-values were determined using linear-mixed effect models (**Table S4**) and volcano plots were generated for data visualization. The X-axis of the plot corresponds to the log2 fold changes of glycan abundance and the y-axis to the negative log2 of the adjusted p-values. The horizontal dashed line represents the threshold of significance α= 0.05. All glycopeaks showing significant differences between baseline and infected time-points are indicated by a colored datapoint (red = increase, blue = decrease). Corresponding *N*-glycan structures are represented using the CFG nomenclature (see **Figure 1** inset), adjacent to the datapoint corresponding to each glycopeak, numbered according to elution in the HILIC-UPLC profile (**Figure 4.A** and **Figure S1**).

Finally, taking advantage of the use of the exact same workflow for both studies, we compared the changes observed in rhesus macaque *N*-glycans during infection with *B. malayi* with the changes in canine serum *N*-glycans during infection with the dog heartworm *Dirofilaria immitis* (*D. immitis*)[51]. We compared the alteration of serum *N*-glycosylation observed at 27 wpi for the dogs and at 15 wpi for the rhesus macaques since these time-points coincide with the microfilariaemic stage of infection for the animals in both studies. Both filarial infections impact the serum *N*-glycosylation and we focused on *N*-glycan structures that were identified in both dog and rhesus macaque serum (**Table S6**). Some similarities could be observed, for instance the abundance of F(6)A2, F(6)A2G1, F(6)A2G2 and F(6)A2G2S_{Gc}1 is increased in both infections, while abundance of F(6)A2G2S_{Gc}2 decreased in both cases. However, several glycan structures were differentially impacted in both studies. As an example, abundance of A2G2S_{Gc}2 decreased in rhesus macaque serum upon microfilariaemia while it increased in dog serum. Thus, we could not highlight a very clear common trend for both filarial infections and our data tends more toward a parasite- and species-specific alteration of the serum *N*-glycome.

Discussion

In this study, we first conducted a comprehensive characterization of rhesus macaque serum *N*-glycans. We used MALDI-TOF-MS analysis and HILIC-UPLC profiling together with glycosidase-based glycan sequencing and available knowledge of mammalian glycosylation pathways[66] to propose the most likely and complete structural assignment of serum and IgG *N*-glycans (**Figures 1-2** and **Table S1** and **S2**). This combination of technologies was highly complementary. Extreme sensitivity of the MALDI-TOF-MS analysis allowed a broad coverage of the serum *N*-glycome structures, while HILIC-UPLC profiling provided quantitative information. The addition of a linkage-specific derivatization of sialic acid was particularly helpful for the analysis of *N*-glycan structures containing these residues. Rhesus macaque serum, like human serum, appeared to be rich in complex, bi to tetra antennary, highly sialylated *N*-glycans. Neu5Gc, a sialic acid not occurring in humans due to the absence of an active CMAH gene, was the major form of sialic acid detected in rhesus macaque serum *N*-glycans, while Neu5Ac was also present in a lower proportion. Absence or presence of Neu5Gc is thought to affect a plethora of biological functions particularly immunity, with differences in susceptibility to pathogens and cell reactivity due for instance to changes in Siglec binding[67] and it is not clear to what extent the effects of Neu5Gc in rhesus macaques mirror those of Neu5Ac in humans. In addition to this major difference between human and rhesus macaque serum *N*-glycosylation, elevated fucosylation levels were also observed in rhesus macaque.

Given its significant contribution to serum *N*-glycans and relevance in immunology, we also examined rhesus macaque IgG *N*-glycans. We observed features expected from the literature such as core-fucosylation of virtually every structure, the presence of Neu5Gc and bisecting GlcNAcs[28,37]. The latter is consistent with a gene homolog of the human beta-1,4-mannosyl-glycoprotein 4-beta-N-acetylglucosaminyltransferase known to exist in rhesus macaques (https://www.ncbi.nlm.nih.gov/, Gene ID: #703643). In addition, some truncated (*e.g.* FA2) and galactosylated *N*-glycans (*e.g.* FA2G1, FA2BG1, FA2G2), major features of human IgG *N*-glycans, were also detected in rhesus macaque IgG *N*-glycans. FA2G1 and FA2BG1 have been reported to be preferentially galactosylated on the α1-6 branch of the *N*-glycan core for both humans and rhesus macaques[28]. Our data corroborated this observation with the ratios of FA2G1 and FA2BG1 respective isomers being almost identical for rhesus macaques and humans (**Figure 3B**) which might be indicative of a highly conserved β-1,4-galactosyltranseferase specificity and activity in both species. Despite these similarities with humans, the *N*-glycan profile of rhesus macaque IgG also showed major differences. In particular, although truncated and galactosylated structures were significantly represented, the major *N*-glycan species found on rhesus macaque IgG was FA2G2S$_{Gc}$1 (HILIC-UPLC glycopeak #14, **Figure S2.A** and **Table S2**). In addition, disialylated complex *N*-glycan structures FA2G2S2 (glycopeak #16), FA2G2S$_{Gc}$2 (glycopeak #18) and FA2BG2S$_{Gc}$2 (glycopeak #19) constitute a significant proportion of rhesus macaque IgG *N*-glycans. Altogether, rhesus macaque IgG has a significantly higher proportion of sialylated *N*-glycans than human IgG. Our results are mostly in line with the characterization of rhesus macaque IgG *N*-glycans conducted previously[28] whereby FA2, FA2G1-2, FA2G1S$_{Gc}$1, FA2G2S$_{Gc}$1-2 were identified as major structures and FA2B, FA2BG1-2, FA2BG1S$_{Gc}$1, FA2BG2S$_{Gc}$1-2 were detected as well albeit in lower amounts. Differences between these findings, in particular the larger number of *N*-glycans identified in our analysis - can easily be explained by improvement of methods and MALDI-TOF-MS technologies over the past decades as well as the use of HILIC-UPLC for quantification in our study, which was not performed earlier[28]. Higher levels of sialylated *N*-glycans were measured for rhesus macaque IgG than for humans in the previous study, matching our observations. However, a significantly lower number of acidic sugars than neutral sugars was found, which appears somewhat contradictory to our results. In addition, only the Neu5Gc form of sialic acids was detected, while we identified 4 HILIC-UPLC glycopeaks and 6 MALDI-TOF-MS ions containing Neu5Ac (**Table S2**). Improved analytics, especially the linkage-specific derivatization of sialic acids, can again easily explain this divergence particularly given the very low abundance of Neu5Ac.

The predominance of the Neu5Gc form of sialic acid in the rhesus macaque *N*-glycan IgG profile raises the question of possible biological implications and immune differences between rhesus macaques and humans. Interestingly, the importance of

sialic acid on *N*-glycans of the IgG Fc region is unclear. Some studies have suggested that sialylation of Fc *N*-glycan is necessary for the IgG anti-inflammatory properties[68,69] while more recent work showed that sialic acid does not affect recognition by Fc γ receptors (FcγRs) III[36,70,71]. Thus, despite major differences in IgG *N*-glycans, including the type of sialic acid, rhesus macaques might have Antibody-Dependent Cellular Toxicity mechanisms that are highly similar to humans. Presence or absence of core-fucosylation, in particular, has been shown to be one of the major mediators of functional changes in IgG for FcgR- and complement-mediated effector functions, together with terminal galactosylation[72,73]. Our analysis showed the presence of both *N*-glycan features on healthy rhesus macaque IgG, which appears in line with the aforementioned hypothesis and strengthens the idea of rhesus macaques as a valid animal model for translation to humans.

We believe that our study contributes to a better knowledge of rhesus macaque serum *N*-glycans which is highly relevant to many studies where they serve as a model for human diseases. Here, we defined the healthy macaque serum *N*-glycoprofile and used it as a baseline to study the changes in *N*-glycosylation during establishment of infection with the parasitic filarial nematode *B. malayi*. This longitudinal serum set did not yield striking visual changes within the serum *N*-glycan profiles such as those that have been observed in infection with the filarial nematode *D. immitis* in dogs[51]. Nonetheless, we highlighted many statistically significant changes between the various post infection time-points and the stable baseline defined by the uninfected profile (**Figure 4**). When focusing on broad classes of glycans, we noted an overall increase of galactosylation and a reduction in sialylation that were similarly reported for *D. immitis* infections[51]. Interestingly, although higher degrees of fucosylation have previously been associated with various disease conditions[74–76] - including during infection with *D. immitis*[51] - we could not observe any clear and statistically significant trend regarding changes in the abundance of fucosylation during primate infection with *B. malayi* (**Figure 5**).

At the individual *N*-glycan level, changes arise early, as soon as 5 wpi, when none of the animals was yet microfilariaemic (**Table S3**). This is consistent with immune responses to parasite (glycan) antigens already occurring at 5 wpi[77]. Surely, given their significant contribution to serum *N*-glycans[1], induction of Igs to *B. malayi* antigens (BmA) may affect the overall profile. In particular, specific IgM to parasite glycans has been observed to appear early during infection (at 5 wpi) and to decrease gradually thereafter[77]. This dynamic of early immune response might explain early changes in the *N*-glycoprofile (*e.g.* glycopeaks #12, 17, 24, **Figure 4**). Nonetheless, most of the changes observed appeared to be “mono-directional” (either increase or decrease) from 5 to 15 wpi, which is an advantage for putative biomarkers. When focusing on the most abundant *N*-glycans (**Figure 6**), structures that appear to decrease upon infection are mostly sialylated complex *N*-glycans while several galactosylated *N*-glycans

increase in relative abundance. This result which was also reflected in the analysis of the changes in glycan classes (**Figure 5**), could possibly be a consequence of an impact of LF on the sialyltransferase or CMAH activity. A critical question to further evaluate is whether those changes would be maintained on the longer term. Indeed, in serum of dogs infected with *D. immitis*, out of the 25 HILIC-UPLC *N*-glycan glycopeaks that were up or down-regulated after 27 weeks of infection – which coincided with the start of microfilaremia production - only 5 were still altered in chronically infected dogs (after 2.5 years of patent infection). Our sample set does not allow us to tackle this question so study of serum from chronically infected animals would be necessary. In addition, our study used a relatively small group of young macaques. Future studies should consider a larger cohort that includes a wider diversity of individuals to address the effect of natural phenomena, such as aging, that might affect the serum *N*-glycan profile[8;9]. Moreover, it would be important to study when the serum *N*-glycan profile returns to normal after anthelmintic treatment of LF – if it ever does.

The origins of the observed changes in serum *N*-glycosylation - resulting from changes in glycan microheterogeneity and/or serum protein composition/relative amount - are of major interest. In humans, over 15 different proteins are thought to contribute to the major *N*-glycan structure of total serum A2G2S2[1], and we might expect something similar for $A2G2S_{Gc}2$ in rhesus macaques. In this study, total IgG glycan microheterogeneity does not appear to be affected by LF unlike observations for many human diseases ranging from cancers to intestinal or liver conditions[76,78,79]. In addition, in both bancroftian LF[52,80] and leishmaniasis[49], differences in IgG Fc *N*-glycosylation have also been identified between different subpopulations of infected individuals (*i.e.* symptomatic or asymptomatic). Unfortunately, our dataset did not allow us to address this question for LF in rhesus macaques since all animals in the cohort were symptomatic (**Table S3**). It would also be of interest to investigate *N*-glycans of *B. malayi* antigen-specific IgG. For many other infectious diseases, antigen-specific IgG Fc glycosylation has indeed shown robust glycosylation profiles between individuals, when total IgG would not, or have been associated with different degree of disease[47].

The observed changes might however originate in part from increased levels of IgG in total serum, as observed in dog serum in response to infection with *D. immitis*. This would be consistent with the fact that many IgG glycopeaks appear to be upregulated at 15 wpi (HILIC-UPLC glycopeaks #1, 5, 6, 7, 9, 12, 14, 16, 19, 21). Nonetheless, this pattern is considerably less pronounced in our study than for *D. immitis* infection in dogs. Thus, it would need confirmation and cannot explain the totality of the changes we observed. Consequently, it would be of great interest to investigate a broader spectrum of serum glycoproteins to address the question of the origin of the observed *N*-glycan alterations. Glycoproteomic studies appear particularly promising in the search for biomarkers. For instance, alpha-1-acid

glycoprotein (AGP), an acute phase glycoprotein in serum has been shown to present alterations of *N*-glycans specific for type-II diabetes or prostate cancer[81,82]. Moreover, multiplying and coupling a selection of diverse molecules (so called panel of biomarkers) has already given very positive results for early detection of hepatocellular carcinoma in humans[83,84]. This could be a strategy to consider here since the large number of altered *N*-glycan structures suggest an impact of LF on more than one serum glycoprotein. This is also consistent with observations of an increase in the circulating levels of various serum glycoproteins being associated with pathogenesis of disease in human LF[85]. In conclusion, we appreciate that the data presented here derive from a small cohort of animals, restricted to the disease establishment period and that further studies are needed to develop serum *N*-glycans as possible biomarkers for infection in humans. Nonetheless, we report a clear effect of disease establishment on the rhesus macaque serum *N*-glycoprofile together with indications of specificity of the observed changes for LF.

Acknowledgements

We acknowledge Mr James Ellard, Drs.Thomas Evans, Richard Roberts and the late Donald Comb of New England Biolabs for their continued support and funding of parasite glycobiology. We acknowledge NIH funding 5 R01 AI116441 used for collecting the rhesus macaque sera.

Data availability

HILIC-UPLC and MALDI-TOF-MS(/MS) spectra supporting our findings have been made available in the supplementary data. In addition, all raw MALDI-TOF-MS and MALDI-TOF-MS/MS data presented in this study (both from main and supplementary figures) have been deposited in Glycopost (https://glycopost.glycosmos.org/, project ID: GPST000274).

Supplementary data

This article contains supplementary data. All supplementary material can be found online with the published article (*10.1038/s41598-022-19964-1*). A selection of supplementary tables and figures is appended at the end of this chapter.

Author contributions

LMCP, CHT, AvD, CHH and JMF: conceptualization; **LMCP, ES, AJB, DLN, MBG:** experimental investigation; **LMCP, ES, AJB:** data analysis; **VK, RK:** resources; **CHT, AvD, CHH and JMF:** supervision; **LMCP, AvD, CHH and JMF:** writing. All authors contributed to revision, editing and approval of the final manuscript.

Conflict of interest

The authors declare no competing interests.

Abbreviations

2-AA	Anthranilic acid	**LF**	Lymphatic filariasis
ACN	Acetronitrile	**MALDI-TOF-MS**	Matrix-assisted laser desorption/ionization time of flight mass spectrometry
AcOH	Acetic acid	**Mf(s)**	Microfilaria(e)
B. malayi	*Brugia malayi*	**MQ**	MilliQ water
B. timori	*Brugia timori*	**MS**	Mass spectrometry
C18	Octyldecylsilane	**MS/MS**	Tandem MS
CMAH	CMP-N-acetylneuraminic acid hydroxylase	**NEB**	New England Biolabs
D. immitis	*Dirofilaria immitis*	**Neu5Ac**	*N*-acetylneuraminic acid
DHB	2,5-dihydroxybenzoic acid	**Neu5Gc**	*N*-glycolylneuraminic acid
DMSO	Dimethyl sulfoxide	**PBS**	Phosphate-buffered saline
EDC	N-(3-Dimethylaminopropyl)-N'-ethylcarbodiimide hydrochloride	**PNGase F**	Peptide-*N*-glycosidase F
FcγRs	Fc g receptors	**SDS**	Sodium dodecyl sulfate
GlcNAc	N-acetylglucosamine	**SPE**	Solid phase extraction
GU	Glucose units	**TFA**	Trifluoroacetic acid
HILIC	Hydrophilic interaction chromatography	**UPLC**	Ultraperformance liquid chromatography
Ig	Immunoglobulin	***W. bancrofti***	*Wuchereria bancrofti*
LF	Lymphatic filariasis	**wpi**	Weeks Post-Infection

References

1. Clerc, F. *et al.* Human plasma protein *N*-glycosylation. *Glycoconj J* **33**, 309–343 (2016).
2. Varki, A. Biological roles of glycans. *Glycobiology* **27**, 3–49 (2017).
3. Aldredge, D., An, H. J., Tang, N., Waddell, K. & Lebrilla, C. B. Annotation of a serum *N*-glycan library for rapid identification of structures. *J Proteome Res* **11**, 1958–1968 (2012).
4. Klein, A. *Human Total Serum* N-*Glycome*. *Advances in Clinical Chemistry* (Advances in Clinical Chemistry, 2008).
5. Ruhaak, L. R. *et al.* Hydrophilic Interaction Chromatography-based high-throughput sample preparation method for *N*-glycan analysis from total human plasma glycoproteins. *Anal Chem* **80**, 6119–6126 (2008).
6. Stockmann, H., O'Flaherty, R., Adamczyk, B., Saldova, R. & Rudd, P. M. Automated, high-throughput serum glycoprofiling platform. *Integrative Biology* **7**, 1026–1032 (2015).
7. Gornik, O. *et al.* Stability of *N*-glycan profiles in human plasma. *Glycobiology* **19**, 1547–1553 (2009).
8. Ding, N. *et al.* Human serum *N*-glycan profiles are age and sex dependent. *Age Ageing* **40**, 568–575 (2011).
9. Gebrehiwot, A. G. *et al.* Healthy human serum *N*-glycan profiling reveals the influence of ethnic variation on the identified cancer-relevant glycan biomarkers. *PLoS One* **13**, 1–23 (2018).
10. Doherty, M. *et al.* Plasma *N* -glycans in colorectal cancer risk. *Sci Rep* **8**, 1–12 (2018).
11. Hu, M., Lan, Y., Lu, A., Ma, X. & Zhang, L. Glycan-based biomarkers for diagnosis of cancers and other diseases: Past, present, and future. in *Progress in Molecular Biology and Translational Science* vol. 162 1–24 (Elsevier Inc., 2019).
12. Kirwan, A., Utratna, M., Dwyer, M. E. O., Joshi, L. & Kilcoyne, M. Glycosylation-based serum biomarkers for cancer diagnostics and prognostics. *Biomed Res Int* **2015**, (2015).
13. Verhelst, X. *et al.* A glycomics-based test predicts the development of hepatocellular carcinoma in cirrhosis. *Clinical Cancer Research* **23**, 2750–2758 (2017).
14. Wittenbecher, C. *et al.* Plasma *N*-glycans as emerging biomarkers of cardiometabolic risk: a prospective investigation in the EPIC-Potsdam Cohort Study. *Diabetes Care* **43**, 1–8 (2020).
15. Reiding, K. R. *et al.* High-throughput serum *N*-glycomics: method comparison and application to study rheumatoid arthritis and pregnancy-associated changes. *Molecular & Cellular Proteomics* **18**, 3–15 (2019).
16. Clerc, F. *et al.* Plasma *N*-glycan signatures are associated with features of inflammatory bowel diseases. *Gastroenterology* **155**, 829–843 (2018).
17. Saldova, R. *et al.* *N*-Glycosylation of serum IgG and total glycoproteins in MAN1B1 deficiency. *J Proteome Res* **14**, 4402–4412 (2015).
18. Xia, B. *et al.* Serum *N*-glycan and *O*-glycan analysis by mass spectrometry for diagnosis of congenital disorders of glycosylation. *Anal Biochem* **442**, 178–185 (2013).

19. Vanderschaeghe, D. *et al.* GlycoFibroTest is a highly performant liver fibrosis biomarker derived from DNA sequencer-based serum protein glycomics. *Molecular & Cellular Proteomics* **8**, 986–994 (2009).

20. Kobata, A. The *N*-linked sugar chains of human immunoglobulin G: their unique pattern, and their functional roles. *Biochim Biophys Acta* **1780**, 472–478 (2008).

21. Gornik, O., Pavi, T. & Lauc, G. Alternative glycosylation modulates function of IgG and other proteins — Implications on evolution and disease. *Biochim Biophys Acta* **1820**, 1318–1326 (2012).

22. Gudelj, I., Lauc, G. & Pezer, M. Immunoglobulin G glycosylation in aging and diseases. *Cell Immunol* **333**, 65–79 (2018).

23. Bondt, A. *et al.* Immunoglobulin G Fab glycosylation analysis using a new mass spectrometric high-throughput profiling method reveals pregnancy-associated changes. *Molecular & Cellular Proteomics* **13**, 3029–3039 (2014).

24. Huhn, C., Selman, M. H. J., Ruhaak, L. R. & Deelder, A. M. IgG glycosylation analysis. *Proteomics* **9**, 882–913 (2009).

25. Stöckmann, H., Adamczyk, B., Hayes, J. & Rudd, P. M. Automated high-throughput IgG-antibody glycoprofiling platform. *Anal Chem* 8841–8849 (2013).

26. Wuhrer, M. *et al.* Glycosylation profiling of IgG subclasses from human serum. *Proteomics* **7**, 4070–4081 (2007).

27. Yuan, W., Sanda, M., Wu, J., Koomen, J. & Goldman, R. Quantitative analysis of immunoglobulin subclasses and subclass specific glycosylation by LC-MS-MRM in Liver Disease. *J Proteomics* **116**, 24–33 (2015).

28. Raju, T. S., Briggs, J. B., Borge, S. M. & Jones, A. J. S. Species-specific variation in glycosylation of IgG: evidence for the species-specific sialylation and branch-specific galactosylation and importance for engineering recombinant glycoprotein therapeutics. *Glycobiology* **10**, 477–486 (2000).

29. Adamczyk, B. *et al.* Comparison of separation techniques for the elucidation of IgG *N*-glycans pooled from healthy mammalian species. *Carbohydr Res* **389**, 174–185 (2014).

30. Hamako, J., Matsui, T., Ozeki, Y., Mizuochi, T. & Titani, K. Comparative studies of asparagine-linked sugar chains of IgG from eleven mammalian species. *Comp Biochem Physiol* **10615**, 949–954 (1993).

31. Blomme, B. *et al.* Alterations of serum protein *N*-glycosylation in two mouse models of chronic liver disease are hepatocyte and not B cell driven. *American Journal of Physiology-Gastrointestinal and Liver Physiology* **300**, G833–G842 (2011).

32. Behrens, A. *et al.* Glycosylation profiling of dog serum reveals differences compared to human serum. *Analytical Glycobiology* **28**, 825–831 (2018).

33. Boesch, A. W., Miles, A. R., Chan, Y. N., Osei-owusu, N. Y. & Ackerman, M. E. IgG Fc variant cross-reactivity between human and rhesus macaque FcgRs. *MAbs* **9**, 455–465 (2017).

34. Phillips, K. A. *et al.* Why primate models matter. *Am J Primatol* **76**, 801–827 (2015).

35. Crowley, A. R. & Ackerman, M. E. Mind the gap: how interspecies variability in IgG and its receptors may complicate comparisons of human and non-human primate effector function. *Front Immunol* **10**, 1–19 (2019).

36. Crowley, A. R. *et al.* Biophysical evaluation of rhesus macaque Fc gamma receptors reveals similar IgG Fc glycoform preferences to human receptors. *Front Immunol* **12**, 1–9 (2021).

37. Mahan, A. E. *et al.* A method for high-throughput, sensitive analysis of IgG Fc and Fab glycosylation by capillary electrophoresis. *J Immunol Methods* **417**, 34–44 (2016).

38. Giambartolomei, G. H., Lasater, B. L., Villinger, F. & Dennis, V. A. Diminished production of T helper 1 cytokines and lack of induction of IL-2R+ T cells correlate with T-cell unresponsiveness in rhesus monkeys chronically infected with *Brugia malayi*. *Exp Parasitol* **90**, 77–85 (1998).

39. Dennis, V. A., Lasater, B. L., Blanchard, J. L., Lowrie, R. C. & Campeau, R. J. Histopathological, lymphoscintigraphical, and immunological changes in the inguinal lymph nodes of rhesus monkeys during the early course of infection with *Brugia malayi*. *Exp Parasitol* **89**, 143–152 (1998).

40. WHO. Lymphatic filariasis - Key Facts. http://www.who.int/mediacentre/factsheets/fs102/en/ (2014).

41. Wanji, S. *et al.* Mapping of lymphatic filariasis in loiasis areas: a new strategy shows no evidence for *Wuchereria bancrofti* endemicity in Cameroon. *PLoS Negl Trop Dis* **13**, 1–15 (2019).

42. Lourens, G. B. & Ferrell, D. K. Lymphatic filariasis. *Nursing Clinics of North America* **54**, 181–192 (2019).

43. Osei-atweneboana, M. Y. *et al.* Phenotypic evidence of emerging ivermectin resistance in *Onchocerca volvulus*. *PLoS Negl Trop Dis* **5**, 1–11 (2011).

44. Taylor, M. J., Hoerauf, A. & Bockarie, M. Lymphatic filariasis and onchocerciasis. *The Lancet* **376**, 1175–1185 (2010).

45. Schwab, A. E., Churcher, T. S., Schwab, A. J. & Prichard, R. K. Population genetics of concurrent selection with albendazole and ivermectin or diethylcarbamazine on the possible spread of albendazole resistance in *Wuchereria bancrofti*. *Parasitology* **133**, 589–601 (2006).

46. Casulli, A. New global targets for NTDs in the WHO roadmap 2021–2030. *PLoS Negl Trop Dis* **15**, 1–10 (2021).

47. Irvine, E. B. & Alter, G. Understanding the role of antibody glycosylation through the lens of severe viral and bacterial diseases. *Glycobiology* **30**, 241–253 (2020).

48. De Jong, S. E. *et al.* IgG1 Fc *N*-glycan galactosylation as a biomarker for immune activation. *Sci Rep* **6**, 1–9 (2016).

49. Gardinassi, L. G. *et al.* Clinical severity of Visceral Leishmaniasis is associated with changes in immunoglobulin Fc *N*-Glycosylation. *mBio* **5**, (2014).

50. Rehan, I. F. *et al.* Sialylated *N*-glycan profile during acute and chronic infections with *Toxoplasma gondii* in mice. *Sci Rep* **10**, 1–17 (2020).

51. Behrens, A. *et al.* Changes in canine serum *N*-glycosylation as a result of infection with the heartworm parasite *Dirofilaria immitis*. *Sci Rep* **8**, 1–9 (2018).

52. O'Regan, N. L. *et al.* Filariasis asymptomatically infected donors have lower levels of disialylated IgG compared to endemic normals. *Parasite Immunol* **36**, 713–720 (2014).

53. Khatri, V., Chauhan, N., Vishnoi, K. & Kalyanasundaram, R. Prospects of developing a prophylactic vaccine against human lymphatic filariasis - evaluation of protection in non-human primates. *Int J Parasitol.* **48**, 773–783 (2019).

54. Reiding, K. R., Blank, D., Kuijper, D. M., Deelder, A. M. & Wuhrer, M. High-throughput profiling of protein glycosylation by MALDI-TOF-MS employing linkage-specific sialic acid esterification. *Anal Chem* **86**, 5784–5793 (2014).

55. De Haan, N. *et al.* Linkage-specific sialic acid derivatization for MALDI-TOF-MS profiling of IgG glycopeptides. *Anal Chem* **87**, 8284–8291 (2015).

56. Selman, M. H. J., Hemayatkar, M., Deelder, M. & Wuhrer, M. Cotton HILIC SPE microtips for microscale purification and enrichment of glycans and glycopeptides. *Anal Chem* **83**, 2492–2499 (2011).

57. Ceroni, A. *et al.* GlycoWorkbench: A tool for the computer-assisted annotation of mass spectra of glycans. *J Proteome Res* **7**, 1650–1659 (2008).

58. Choi, M. *et al.* MSstats: An R package for statistical analysis of quantitative mass spectrometry-based proteomic experiments. *Bioinformatics* **30**, 2524–2526 (2014).

59. Powell, A. K. & Harvey, D. J. Stabilization of sialic acids in *N*-linked oligosaccharides and gangliosides for analysis by positive ion matrix-assisted laser desorption/ionization mass spectrometry. *Rapid Communications in Mass Spectrometry* **10**, 1027–1032 (1996).

60. Chou, H.-H. *et al.* A mutation in human CMP-sialic acid hydroxylase occurred after the Homo-Pan divergence. *Proc Natl Acad Sci U S A* **95**, 11751–11756 (1998).

61. Hedlund, M. *et al. N*-Glycolylneuraminic acid deficiency in mice: implications for human biology and evolution. *Mol Cell Biol* **27**, 4340–4346 (2007).

62. Bergfeld, A. K., Pearce, O. M. T., Diaz, S. L., Pham, T. & Varki, A. Metabolism of vertebrate amino sugars with *N*-Glycolyl groups: Elucidating the intracellular fate of the non-human sialic acid N-glycolylneuraminic. *J Biol Chem* **287**, 28865–28881 (2012).

63. Davies, L. R. L. *et al.* Metabolism of vertebrate amino sugars with *N*-Glycolyl-Resistance of alpha2-8-linked *N*-glycolylneuraminic acid to enzymatic cleavage. *J Biol Chem* **287**, 28917–28931 (2012).

64. Peri, S., Kulkarni, A., Feyertag, F., Berninsone, P. M. & Alvarez-ponce, D. Phylogenetic distribution of CMP-Neu5Ac Hydroxylase (CMAH), the enzyme synthetizing the proinflammatory human xenoantigen Neu5Gc. *Genome Biol Evol* **10**, 207–219 (2018).

65. Springer, S. A. & Gagneux, P. Glycomics: revealing the dynamic ecology and evolution of sugar molecules. *J Proteomics* **135**, 90–100 (2016).

66. Stanley, P., Taniguchi, N. & Aebi, M. Chapter 9 N-glycans. in *Essentials of glycobiology 3rd Edition* (ed. Cold Spring Harbor Laboratory Press) doi:10.1101/glycobiology.3e.009.

67. Okerblom, J. & Varki, A. Biochemical, cellular, physiological, and pathological consequences of human loss of N-glycolylneuraminic acid. *ChemBioChem* **18**, 1155–1171 (2017).

68. Kaneko, Y., Nimmerjahn, F. & Ravetch, J. V. Anti-inflammatory activity of Immunoglobulin G resulting from Fc sialylation. *Science (1979)* **313**, 670–673 (2006).

69. Anthony, R. M. *et al.* A recombinant IgG Fc that recapitulates the anti-inflammatory activity of Ivig. *Science (1979)* **320**, 373–376 (2009).

70. Yu, X. *et al.* Engineering hydrophobic protein−carbohydrate interactions to fine-tune mAbs. *J Am Chem Soc* **135**, 9723–9732 (2013).

71. Subedi, G. P. & Barb, A. W. The immunoglobulin G1 *N*-glycan composition affects binding to each low affinity Fc γ receptor Fc g receptor. *MAbs* **8**, 1512–1524 (2016).

72. Dekkers, G., Treffers, L., Plomp, R. & Bentlage, A. E. H. Decoding the human IgG glycan repertoire reveals a spectrum of Fc-Receptor- and complement-mediated effector activities. *Front Immunol* **8**, 1–16 (2017).

73. Kiyoshi, M. *et al.* Assessing the heterogeneity of the Fc-glycan of a therapeutic antibody using an engineered Fc γ Receptor IIIa-immobilized column. *Sci Rep* **8**, 1–11 (2018).

74. Callewaert, N., Schollen, E. & Vanhecke, A. Increased fucosylation and reduced branching of serum glycoprotein *N*-glycans in all known subtypes of congenital disorder of glycosylation I. *Glycobiology* **13**, 367–375 (2003).

75. Comunale, M. A. *et al.* Identification and development of fucosylated glycoproteins as biomarkers of primary hepatocellular carcinoma. *J Proteome Res* **8**, 595–602 (2009).

76. Reily, C., Stewart, T. J., Renfrow, M. B. & Novak, J. Glycosylation in health and disease. *Nat Rev Nephrol* **15**, (2019).

77. Petralia, L. M. C. *et al.* Mass spectrometric and glycan microarray-based characterization of the filarial nematode *Brugia malayi* glycome reveals anionic and zwitterionic glycan antigens. *Molecular & Cellular Proteomics* **21**, 1–22 (2022).

78. Klein, A., Carre, Y., Louvet, A., Michalski, J.-C. & Morelle, W. Immunoglobulins are the major glycoproteins involved in the modifications of total serum *N*-glycome in cirrhotic patients. *Proteomics* **4**, 379–393 (2010).

79. Mehta, A. S. *et al.* Increased levels of galactose-deficient anti-Gal Immunoglobulin G in the sera of hepatitis C virus-infected individuals with fibrosis and cirrhosis. *J Virol* **82**, 1259–1270 (2008).

80. Adjobimey, T. & Hoerauf, A. Distinct *N*-Linked IgG glycosylation patterns are associated with chronic pathology and asymptomatic infections in human Lymphatic Filariasis. *Front Immunol* **13**, 1–12 (2022).

81. Matsumoto, T., Ha, S., Yoneyama, T. & Tobisawa, Y. Serum *N*-glycan profiling is a potential biomarker for castration- resistant prostate cancer. *Sci Rep* **9**, 1–8 (2019).

82. Keser, T. *et al.* High-throughput and site-specific *N*-glycosylation analysis of human alpha-1-acid glycoprotein offers a great potential for new biomarker discovery. *Molecular & Cellular Proteomics* **20**, 0–15 (2021).

83. Black, A. P. & Mehta, A. S. The search for biomarkers of hepatocellular carcinoma and the impact on patient outcome. *Curr Opin Pharmacol* **41**, 74–78 (2018).

84. Parikh, N. D. *et al.* Biomarkers for the early detection of hepatocellular carcinoma. *Cancer Epidemiology, Biomarkers & Prevention* **29**, 2495–2503 (2020).

85. Anuradha, R. *et al.* Circulating microbial products and acute phase proteins as markers of pathogenesis in lymphatic filarial disease. *PLoS Pathog* **8**, 1–9 (2012).

Supplementary material

Supplementary Tables

Table S1 (simplified): Rhesus macaque serum *N*-glycans

Peak # [1] UPLC [1a]	Peak # [1] MALDI [1b]	Theoretical m/z [2]	Composition [3]	Glycans (Oxford Notation Name)	Exoglycosidase digestions [4] Fucosidase	EndoH	β-GlcNAcAse	β-galactosidase	Neuraminidase	Most probable structural assignment [5]	IgG glycan [6]
-	1	1192.43	H4N2	M4	ns	s	ns	ns	ns		
-	2	1233.45	H3N3	A1	ns	ns	-1N	ns	ns		
-	4	1379.51	F1H3N3	F(6)A1	-1F	ns	-1N	ns	ns		
-	5	1395.51	H4N3	A1G1	ns	ns	ns	-1H	ns		
-	6	1436.53	H3N4	A2	ns	ns	-2N	ns	ns		
1	9	1557.56	H5N3	Hybrid M4A1G1	ns	s	ns	-1H	ns		
	10	1582.59	F1H3N4	F(6)A2	-1F	ns	-2N	ns	ns		1
2	8	1541.56	F1H4N3	F(6)A1G1	-1F	ns	ns	-1H	ns		2
3	3	1354.48	H5N2	M5	ns	s	ns	ns	ns		2
	11	1598.58	H4N4	A2G1	ns	ns	-1N	-1H	ns		2
-	12	1639.61	H3N5	A3 or A2B	ns	ns	-3N	ns	ns		
4	14	1686.60 1715.60	H4N3S1	A1G1S1	ns	ns	ns	ns	-1S		3
	15	1702.60 1721.60	H4N3S1	A1G1S_{Gc}1(3)	ns	ns	ns	ns	-1S		3
	16	1719.61	H6N3	Hybrid M5A1G1	ns	s	ns	-1H	ns		

5	17	1744.64	F1H4N4	F(6)A2G1	-1F	ns	-1N	-1H	ns		3
6	17	1744.64	F1H4N4	F(6)A2G1	-1F	ns	-1N	-1H	ns		4
7	24	1947.72	F1H4N5	F(6)A2BG1	-1F	ns	-2N	-1H	ns		5
	20	1801.66	H4N5	A2BG1	ns	ns	-2N	-1H	ns		
8	24	1947.72	F1H4N5	F(6)A2BG1	ns	ns	-2N	-1H	ns		6
	7	1516.53	H6N2	M6	ns	s	ns	ns	ns		6
9	18	1760.64	H5N4	A2G2	ns	ns	ns	-2H	ns		7
	19	1785.67	F1H3N5	F(6)A2B F(6)A3	-1F	ns	-3N	-3H	ns		7
-	26	1963.72	H5N5	A2BG2	ns	ns	ns	-2H	ns		
10	22	1848.65 1877.65	F1H4N3S1	F(6)A1G1S$_{Gc}$(3)1	-1F	ns	ns	ns	-1S		
11	22	1848.65 1877.65	H5N3S1	Hybrid M4A1G1S1	ns	ns	ns	ns	-1S		
	23	1864.65	H5N3S1	Hybrid M4A1G1S$_{Gc}$1	ns	ns	ns	ns	-1S		
12	24	1906.70	F1H5N4	F(6)A2G2	-1F	ns	ns	-2H	ns		8
13	30	2109.77	F1H5N5	F(6)A2BG2	-1F	ns	ns	-2H	ns		9
14	-	1934.67	H4N4S1	A2G1S$_{Gc}$(6)1	ns	ns	ns	ns	-1S		9
15	13	1678.58	H7N2	M7	ns	s	ns	ns	ns		
16	28	2051.73 2080.73	H5N4S1	A2G2S1	ns	ns	ns	-1H	-1S		10
			F1H4N4S1	F(6)A2G1S$_{Gc}$1	-1F	ns	ns	ns	-1S		11

17	29	2067.72 2096.73	H5N4S1	$A2G2S_{Gc}1$	ns	ns	ns	-1H	-1S	
	31	2197.79	F1H5N4S1	F(6)A2G2S(6)1	-1F	ns	ns	-1H	-1S	12. 13
18	33	2254.81 2283.81	H5N5S1	A3G2S(3)1	ns	ns	ns	-1H	-1S	
			F1H4N5S1	$F(6)A2BG1S_{Gc}1$	-1F	ns	-2N	ns	-1S	14
19	32	2212. 79 2213.79 2242.79	F1H5N4S1	$F(6)A2G2S_{Gc}1$	-1F	ns	ns	-1H	-1S	14
-	21	1840.64	H8N2	M8	ns	s	ns	ns	ns	
20	34	2270.81 2299.81	H5N5S1	$A3G2S_{Gc}1$	ns	ns	ns	-1H	-1S	
-	35	2312.85	F1H5N6	F(6)A4G2	-1F	ns	-2N	-2H	ns	
-	36	2328.85	H6N6	A4G3	ns	ns	-1N	-3H	ns	
21	38	2416.87 2445.87	F1H5N5S1	$A2BG2S_{Gc}1$	-1F	ns	ns	-1H	-1S	15
22	-	2371.83	H5N4S2	A2G2S2	ns	ns	ns	ns	-2S	
-	27	2002.69	H9N2	M9	ns	s	ns	ns	ns	
23	40	2488.89	F1H5N4S2	F(6)A2G2S2	-1F	ns	ns	ns	-2S	16
	37	2374.82 2403.06 2432.86	H5N4S2	$A2G2S_{Gc}2$	ns	ns	ns	ns	-2S	17
24	42	2577.90 2634.89	H5N5S2	$A2G3S_{Gc}1$	ns	ns	ns	ns	-2S	18
25	41	2520.88 2549.88 2578.88	F1H5N4S2	$F(6)A2G2S_{Gc}2$	-1F	ns	ns	ns	-2S	18
26	43	2723.96 2781.30	F1H5N5S2	$F(6)A2BG2S_{Gc}1$	-1F	ns	ns	ns	-2S	19

27	39	2432.86	H6N5S1	A3G3S$_{Gc}$1	ns	ns	ns	-2H	-1S	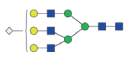
28	-	-	H6N5S2	A3G3S2	ns	ns	ns	-1H	-2S	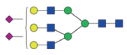
29	44	2739.95 2768.95 2797.95	H6N5S2	A3G3S$_{Gc}$2	ns	ns	ns	-1H	-2S	
30	-	2886.01 2915.01 2944.01	F1H6N5S2	F(6)A3G3S$_{Gc}$2	-1F	ns	ns	-1H	-2S	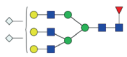
31	-		H7N5S2	A3G4S1S$_{Gc}$1	ns	ns	ns	ns	-2S	
32	-	-	F1H7N5S2	F(6)A3G4S1S$_{Gc}$1	-1F	ns	ns	ns	-2S	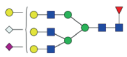
33	-	3057.10	H6N5S3	A3G3S3	ns	ns	ns	ns	-3S	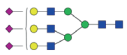
34	45	3047.04	H6N5S3	A3G3S$_{Gc}$3	ns	ns	ns	ns	-3S	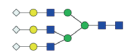
35	-	3073.10 3102.10 3131.10	H7N6S2	A4G4S2	ns	ns	ns	ns	-2S	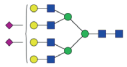
	-		F1H6N6S2	F(6)A4G3S1S$_{Gc}$1	-1F	ns	ns	ns	-2S	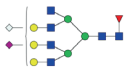
36	-	3193.10	F1H6N5S3	F(6)A3G3S$_{Gc}$3	-1F	ns	ns	ns	-3S	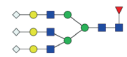
37	-	3250.12	H6N6S3	A4G3S3	ns	ns	-1N	ns	-3S	
38	-	3280.14	H8N6S2	A4G5S1S$_{Gc}$1	ns	ns	ns	ns	-2S	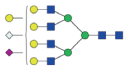
39 - 43	-	3412.17 3441.17 3470.17 3499.17 3748.26 3836.32 3777.26 3865.32	F(0-1) H7(or more) N6(or more) S(3-4)	Multiantennary structures	-0/1F	ns	ns	-1/2H	-3/4S	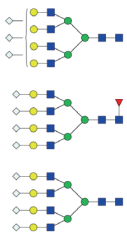

[1]**Peak #:** "glycopeak" number as defined in the HILIC-UPLC (a) and MALDI-TOF-MS (b) profiles of rhesus macaque serum (see **Figure S1**)

[2]**Theoretical *m/z*:** theoretical monoisotopic mass in negative-ion mode (*m/z* [M-H]$^-$) with 2-AA as terminal end modification
[3]**Compositions** were initially deduced by combining HILIC-UPLC results with MALDI-TOF-MS analysis and using the glycopeakfinder tool of Glycoworkbench™ with literature data. They were further confirmed using glycan sequencing (exoglycosidase digestions and MS/MS analysis). H = hexose, N = N-acetylhexosamine, F = fucose, S = Sialic acid
[4]**Exoglycosidase digestions:** effect of exoglycosidase treatment on corresponding *N*-glycan, -nH/N/S = loss of n H/N/S, ns = non-sensitive. S = sensitive and fully digested by the enzyme. Fucosidase = α1-2,4,6 Fucosidase O; EndoH = Endoglycosidase H, β-GlcNAcAse = β-N-Acetylglucosaminidase S, Neuraminidase = α2-3,6,8,9 Neuraminidase A (see **Table S7** below).
MALDI-TOF-MS spectra and HILIC-UPLC profiles of the corresponding glycosidase treatments are shown in **Figures S2-S3** for total serum and in **Figures S5-S6** for IgG.
[5]**Most probable structural assignment** drawn using the CFG nomenclature (see symbol key below).
[6]**IgG glycan** indicates whether the structure has also been identified on IgG *N*-glycans. If so, corresponding HILIC-UPLC peak # as defined in **Figure S4** is specified. Details on the structural characterization of IgG *N*-glycans can be found in **Table S2** online.
An extended version of **Table S1** is available online.

Symbol key:

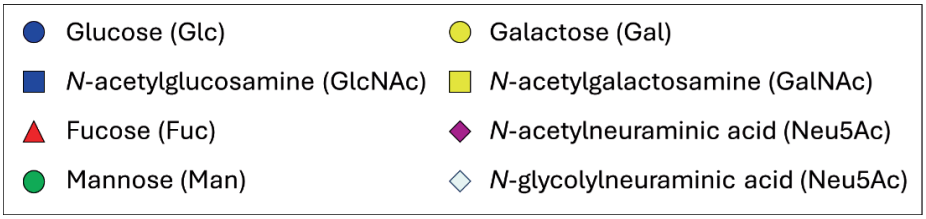

Table S3: Information on *B. malayi*-infected rhesus macaques (longitudinal cohort)

Animal ID	Age (months)[1]	Sex	Microfilaremia 5 wpi[2]		Microfilaremia 12 wpi		Microfilaremia 15 wpi		
			[3]Visual?	[4]Mfs/mL	[3]Visual?	[4]Mfs/mL	[3]Visual?	[4]Mfs/mL	Lymph flow
255	42	Female	No	0	Yes	0	Yes	105	Impaired
256	46	Female	No	0	Yes	5	Yes	10	Impaired
262	62	Male	No	0	Yes	0	Yes	25	Impaired
265	54	Female	No	0	Yes	5	Yes	435	Impaired
298	52	Male	N/A	N/A	N/A	N/A	N/A	N/A	N/A
300	40	Male	N/A	N/A	N/A	N/A	N/A	N/A	N/A
303	48	Male	N/A	N/A	N/A	N/A	N/A	N/A	N/A

[1]Age of animal when initial sample was collected, [2]wpi = weeks post-infection, [3]Microfilaremia visualized using Knott Test on night blood, [4]Mfs/mL = Microfilaria (Mf) count in day blood (as detailed in[53]) in microfilariae (Mfs) per mL.

Table S6: Comparison of *N*-glycan profile alterations in filarial infections

***N*-glycans**		**UPLC peak #[2]**		**Changes during filarial infection (after microfilariaemia)[3]**	
Putative structure[1]	**Glycans (Oxford Notation Name)**	**Dogs infected with *D. immitis* [2a]**	**Macaques infected with *B. malayi* [2b]**	**Dogs infected with *D. immitis***	**Macaques infected with *B. malayi***
	F(6)A2	5	1	Increase	Increase
	F(6)A1G1	6	2	None	Increase
 	M5 A2G1	7, 8, 9	3	Increase (8, 9)	Increase
	F(6)A2G1	10	5	None	Increase
	F(6)A2G1	11, 12	6	Increase	Increase
 	M6 A2G2	13, 14	8, 9	Decrease (13) Increase (14)	Increase
	F(6)A2G2	16, 17	12	Increase	Increase
 	M7 F(6)A2G1SGc1	20	15, 16	None	Increase
	A2G2S1	21, 22	16	None	Increase
	F(6)A2G2S(6)1	23	17	Increase	None
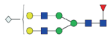	F(6)A2G2S_{Gc}1	28	19	Increase	Increase
	A2G2S2	25, 29, 30	22	Decrease	Increase
	F(6)A2G2S2	31, 32	23	Increase (31) Decrease (32)	Decrease

	A2G2S$_{Gc}$2	34	23	Increase	Decrease
	F(6)A2G2S$_{Gc}$2	36	25	Decrease	Decrease

[1]**Putative structure:** represented using the CFG nomenclature (see **Table S1** above).
[2]**UPLC peak #:** "glycopeak" number as defined in the HILIC-UPLC profiles of rhesus macaque serum *N*-glycans (a = present study) and of dog serum *N*-glycans (b = data from[51])
[3]**Changes during filarial infection:** alteration of serum *N*-glycosylation observed at 27 wpi for the dogs infected with *D. immitis* and at 15 wpi for rhesus macaques infected with *B. malayi*. Increase or decrease in relative abundance were determined by HILIC-UPLC analysis in the present study and in[51].

Table S7: Glycosidases used for glycan sequencing

Enzyme Name	Amount used per reaction[1]		Reaction buffer[2]	Cat. #[3]	Enzyme Source
	Sequen-tial	Non-sequential			
β-N-Acetyl glucosaminidase S	-	2 U	P0744	P0744	*Streptococcus pneumoniae,* recombinant expr. in *E. coli*
Endoglycosidase H	-	1000 U	P0702	P0702	*Streptomyces picatus* and overexpressed in *E. coli*
α1-2,4,6 Fucosidase O	4 U	8 U	P0749	P0749	*Omnitrophica bacterium* recombinant expr. in *E. coli*
α1-3,4,6 Galactosidase	4 U	8 U	P0747	P0747	*Green coffee bean,* recombinant expr. in *E. coli*
β1-4 Galactosidase S	8 U	16 U	P0745	P0745	*Streptococcus pneumoniae,* recombinant expr. in *E. coli*
α2-3,6,8,9 Neuraminidase A	20 U	20 U	P0722	P0722	*Arthrobacter ureafaciens* recombinant expr. in *E. coli*
α2-3 Neuraminidase S	-	16 U	P0743	P0743	*Streptococcus pneumoniae,* recombinant expr. in *E. coli*

All enzymes were obtained from New England Biolabs (NEB).
[1]Amount used per reaction in units (U). U values are based on the provider (NEB) definition
[2]Glycobuffers = reaction buffers provided by NEB; Gb1 = Glycobuffer 1(5 mM CaCl2, 50 mM sodium acetate, pH 5.5 @ 25°C); Gb3 = Glycobuffer 3 (50 mM sodium acetate, pH 6 @ 25°C)
[3]NEB catalog number

Additional supplementary tables online: (https://doi.org/10.1038/s41598-022-19964-1)

- Extended versions of **Table S1:** Rhesus macaque serum *N*-glycans
- **Table S2:** Rhesus macaque IgG *N*-glycans
- **Table S4:** Longitudinal rhesus macaque set (HILIC-UPLC raw data & statistics)
- **Table S5:** Longitudinal rhesus macaque set, glycan classes (HILIC-UPLC raw data & statistics)

Supplementary Figures

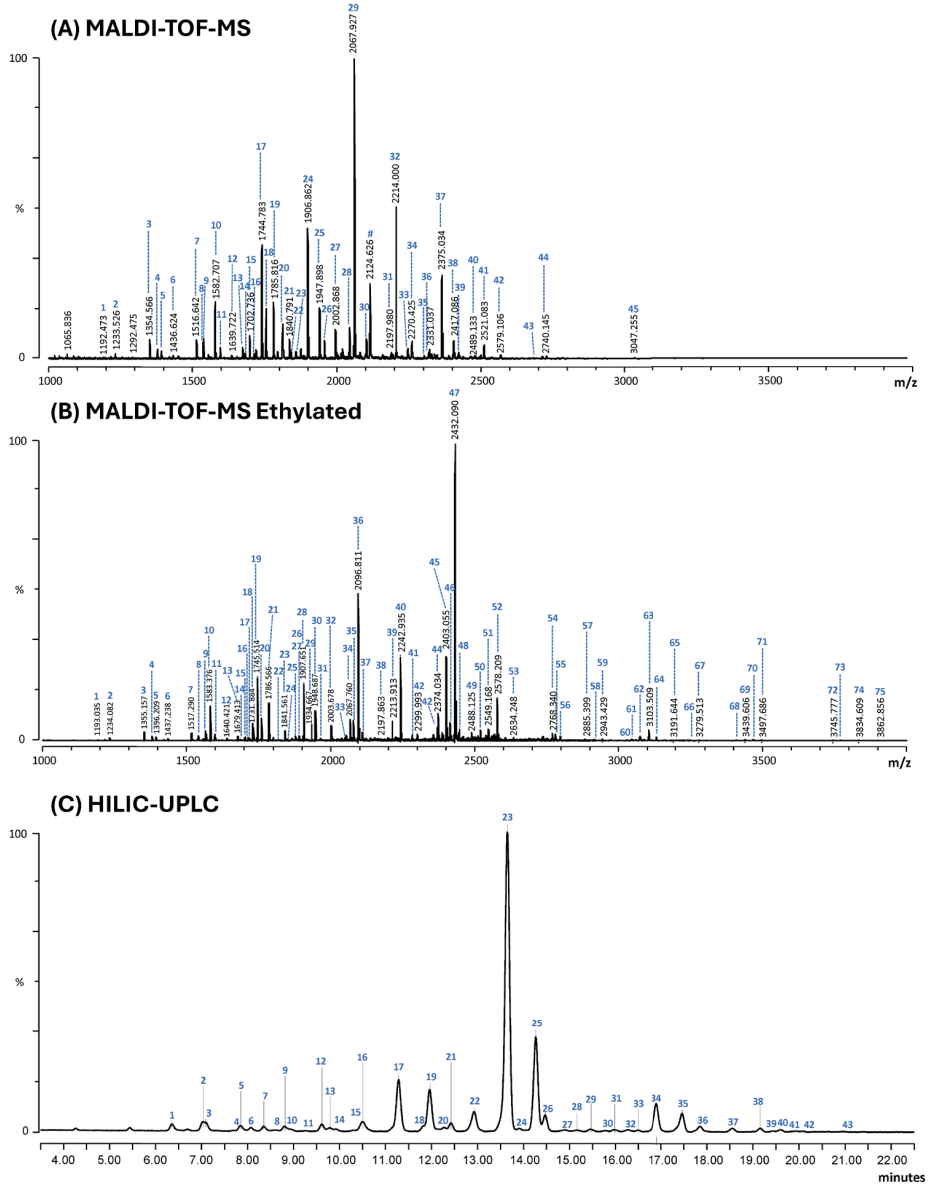

Figure S1: Glycopeak assignment of MALDI-TOF-MS spectra (A and B) and HILIC-UPLC profile (C) of rhesus macaque serum *N*-glycans. *N*-glycans were released from serum glycoproteins using PNGase F and labeled using 2-AA (A, B) or procainamide (C). *N*-glycans were analyzed using MALDI-TOF-MS (A, B) or HILIC-UPLC (C). 43 glycopeaks were detected in the HILIC-UPLC profile and are labeled according to their elution time. In (B), *N*-glycans were subjected to a step consisting of linkage-specific derivatization of the sialic acids by ethyl esterification prior to 2-AA labeling. MALDI-TOF-MS signals to which a glycan structure could be associated and characterized are numbered above the monoisotopic masses. Corresponding glycan structures are depicted in **Table S1** above.

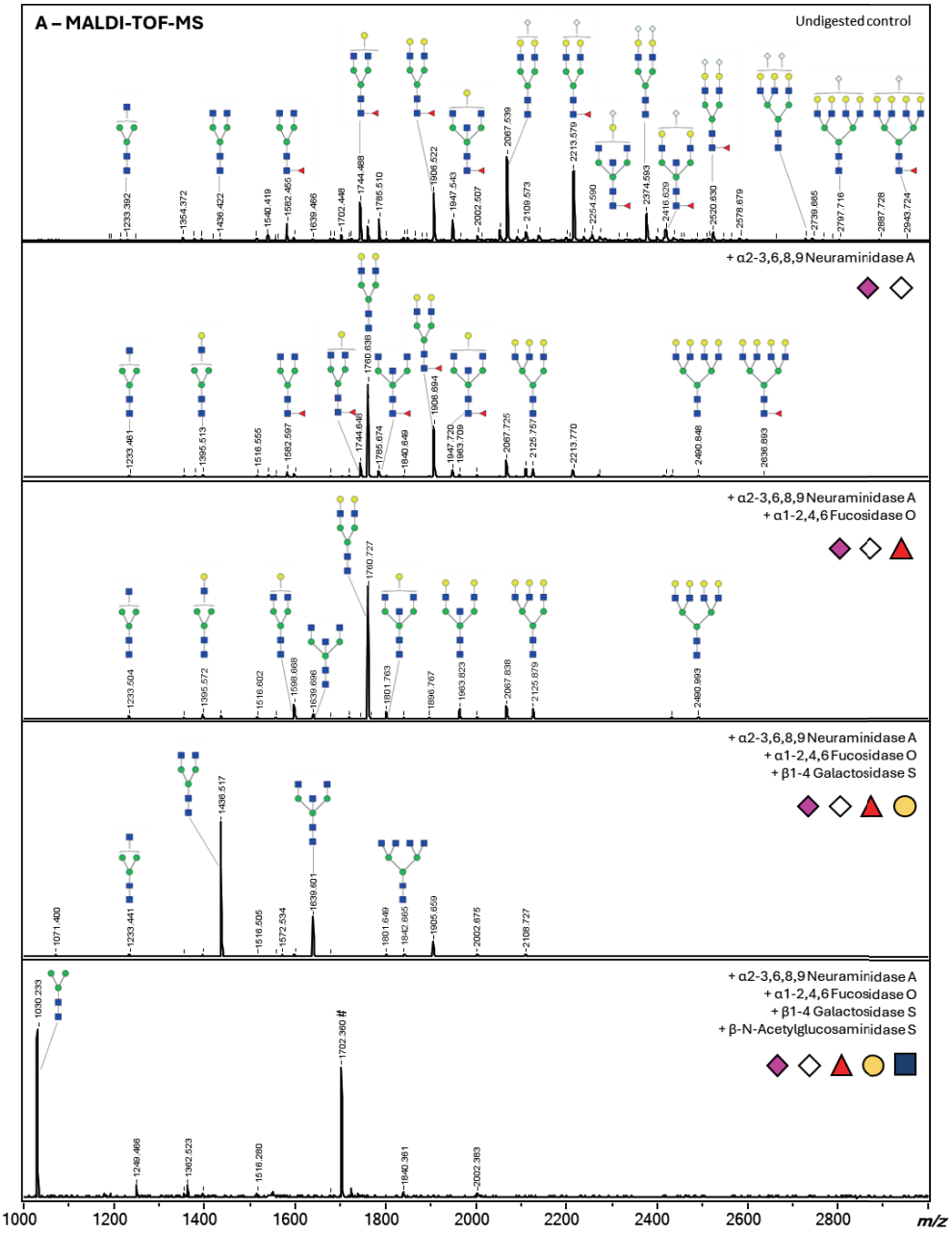

Figure S2: Sequential digestion panel of rhesus macaque serum *N*-glycans. PNGase F released and 2-AA (A) or procainamide (B) labeled *N*-glycans were digested using selected exoglycosidases. The *N*-glycan pool was digested in 4 different reactions containing the following enzymes as indicated: α2-3,6,8,9 Neuraminidase A, α1-2,4,6 Fucosidase O, β1-4 Galactosidase and β-N-Acetylglucosaminidase (see **Table S7**). The reactions progressed from Neuraminidase A alone to a reaction containing all 4 listed

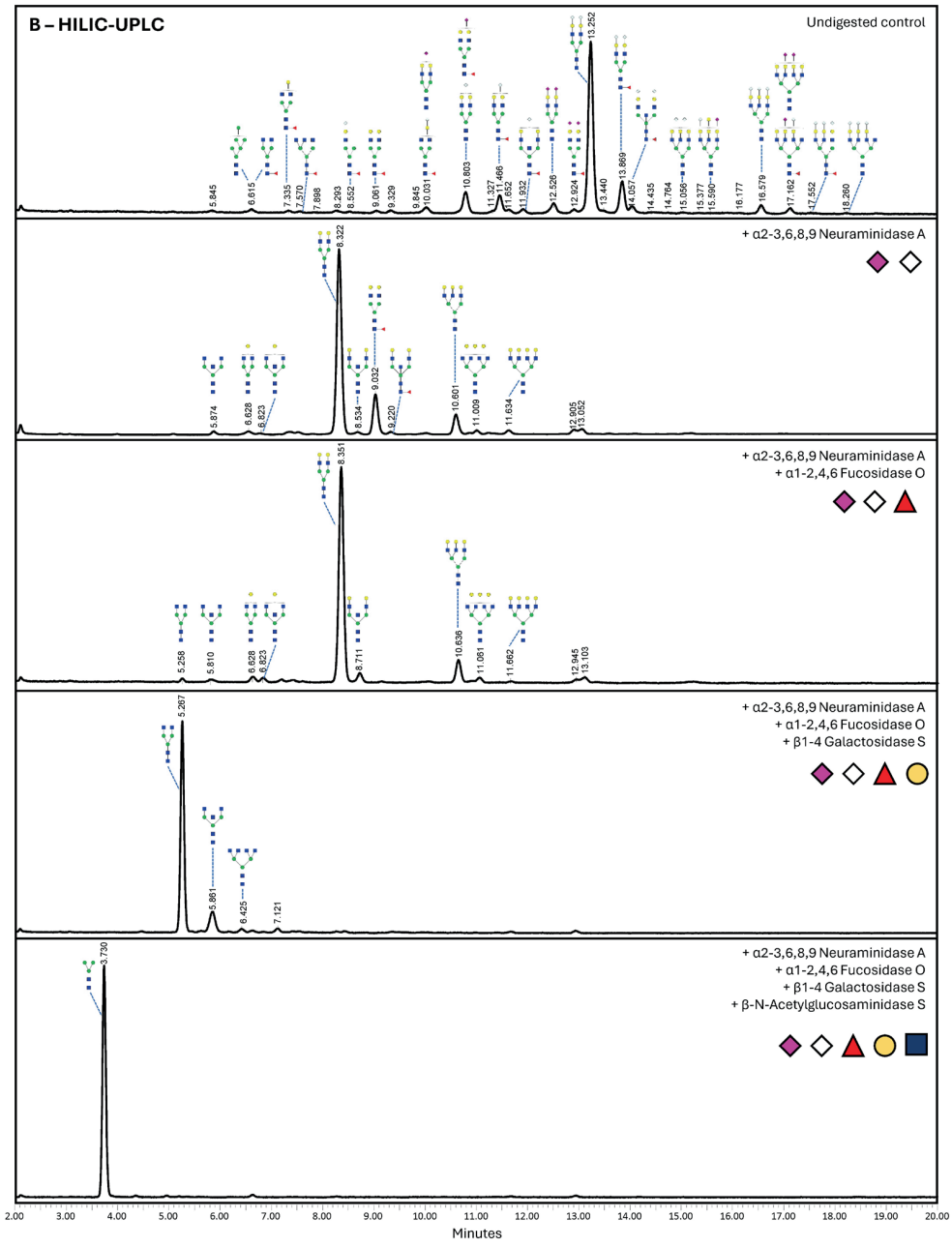

Figure S2. ***(continued)*** enzymes. Digested *N*-glycan samples were measured by MALDI-TOF-MS (A) or analyzed using HILIC-UPLC (B). The upper panel shows the non-digested *N*-glycan pool processed as a control along with the digestions using identical reaction conditions. Non-sequential digestions were additionally performed (**Figure S3**).

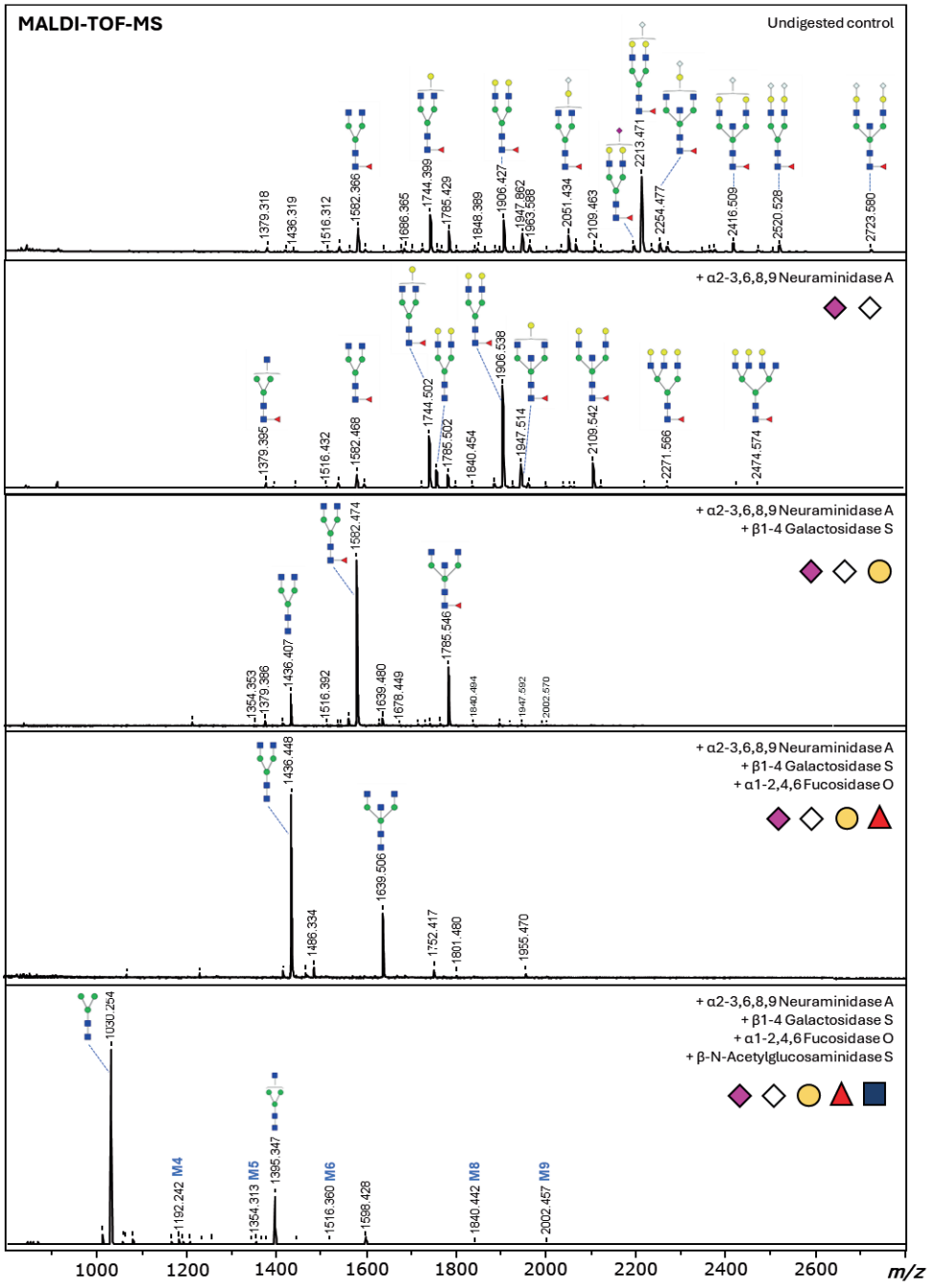

Figure S5: Sequential digestion panel of rhesus macaque IgG *N*-glycans. PNGase F-released and 2-AA-labeled *N*-glycans were digested using selected exoglycosidases. The *N*-glycan pool was digested in 4 different reactions containing the following enzymes as indicated: α2-3,6,8,9 Neuraminidase A, α1-2,4,6

Fucosidase O, β1-4 Galactosidase and β-N-Acetylglucosaminidase (see **Table S7**). The reactions progressed from neuraminidase A alone to a reaction containing all 4 listed enzymes. Digested *N*-glycan samples were measured by MALDI-TOF-MS. The upper panel shows the non-digested *N*-glycan pool processed as a control along with the digestions using identical reaction conditions. Note that the digestion with the β-N-Acetylglucosaminidase (panel 5) was not complete (residual peak with *m/z* = 1395.347 $[M - H]^-$). Non-sequential digestions were additionally performed (**Figure S6**).

Additional supplementary figures online: (https://doi.org/10.1038/s41598-022-19964-1)

- **Figure S3:** Sensitivity of rhesus macaque serum *N*-glycans to individual glycosidase treatments
- **Figure S4:** Glycopeak assignment of MALDI-TOF-MS spectra and HILIC-UPLC profile of rhesus macaque IgG *N*-glycans
- **Figure S6:** Sensitivity of rhesus macaque IgG *N*-glycans to individual glycosidase treatments
- **Figure S7:** (Individual) HILIC-UPLC profiles of uninfected rhesus macaque serum *N*-glycans